Stem Cell Reports
Article

OPEN ACCESS

Hippocampal TERT Regulates Spatial Memory Formation through Modulation of Neural Development

Qi-Gang Zhou,[1,2,*] Meng-Ying Liu,[1] Han-Woong Lee,[3] Fuyuki Ishikawa,[4] Sushil Devkota,[3] Xin-Ru Shen,[1] Xin Jin,[1] Hai-Yin Wu,[1] Zhigang Liu,[2] Xiao Liu,[5] Xun Jin,[2,6] Hai-Hui Zhou,[1] Eun Jeoung Ro,[2] Jing Zhang,[1] Yu Zhang,[1] Yu-Hui Lin,[1] Hoonkyo Suh,[2,*] and Dong-Ya Zhu[1,*]

[1]Department of Clinical Pharmacology, Institution of Stem Cells and Neuroregeneration, Pharmacy College, Nanjing Medical University, Nanjing 211166, P.R. China
[2]Department of Stem Cell Biology and Regenerative Medicine, Lerner Research Institute, Cleveland Clinic, Cleveland, OH 44195, USA
[3]Department of Biochemistry, College of Life Science and Biotechnology, Yonsei Laboratory Animal Research Center, Yonsei University, Seoul 120-749, Korea
[4]Departments of Gene Mechanisms, Graduate School of Biostudies, Kyoto University, Kyoto 606-850, Japan
[5]Department of Chinese Medicine, College of Pharmacy, Nanjing University of Chinese Medicine, Nanjing 210023, P.R. China
[6]Department of Neurosurgery, First Affiliated Hospital of Wenzhou Medical University, Wenzhou, 325015 Zhejiang, P.R. China
*Correspondence: dyzhu@njmu.edu.cn (D.-Y.Z.), qigangzhou@njmu.edu.cn (Q.-G.Z.), suhh2@ccf.org (H.S.)
http://dx.doi.org/10.1016/j.stemcr.2017.06.014

SUMMARY

The molecular mechanism of memory formation remains a mystery. Here, we show that TERT, the catalytic subunit of telomerase, gene knockout (*Tert*$^{-/-}$) causes extremely poor ability in spatial memory formation. Knockdown of TERT in the dentate gyrus of adult hippocampus impairs spatial memory processes, while overexpression facilitates it. We find that TERT plays a critical role in neural development including dendritic development and neuritogenesis of hippocampal newborn neurons. A monosynaptic pseudotyped rabies virus retrograde tracing method shows that TERT is required for neural circuit integration of hippocampal newborn neurons. Interestingly, TERT regulated neural development and spatial memory formation in a reverse transcription activity-independent manner. Using X-ray irradiation, we find that hippocampal newborn neurons mediate the modulation of spatial memory processes by TERT. These observations reveal an important function of TERT through a non-canonical pathway and encourage the development of a TERT-based strategy to treat neurological disease-associated memory impairment.

INTRODUCTION

Telomerase is found to maintain the telomere length by adding DNA bases to the end of the chromosomes for protecting genetic material. Telomerase is a ribonucleoprotein with reverse transcriptase activity that consists of telomerase RNA (TERC) and TERT, a reverse transcriptase (Blackburn, 2001; Nandakumar and Cech, 2013; Zhao et al., 2009). Telomerase is essential for the prolonged persistence of stem cell function in organs with extensive cell turnover (Rufer et al., 1999; Sarin et al., 2005; Wege and Brummendorf, 2007). Besides embryonic and cancer stem cells, proliferative neural stem cells (NSCs) also exhibit high levels of telomerase activity (Cai et al., 2002; Caporaso et al., 2003; Ferron et al., 2004, 2009). To date, the main role of TERT found in NSCs is to regulate proliferation (Zhou et al., 2011). Accordingly, in contrast to the well-studied functions of TERT in embryonic and cancer stem cells (Harley, 2008), still little is known about the function of TERT in NSCs, especially in adult hippocampal dentate gyrus (DG).

The adult brain has the ability to change its structure and function during maturation, learning, environmental challenges, or pathology (Lledo et al., 2006). The adult hippocampus, a crucial structure for the formation of certain types of memory, such as episodic memory and spatial memory (Squire, 1992b), is one of the most plastic regions in the mammalian brain. New neurons are generated continuously throughout life in the DG originating from neural progenitor cells (NPCs) (Ayala et al., 2007). The DG, which receives direct inputs from the entorhinal cortex and sends projections to the CA3 region, is traditionally considered as the information gateway to the hippocampus (Deng et al., 2010; Jaffe and Gutierrez, 2007). The development of a dendritic tree allows newborn neurons to communicate with each other by joining circuits (Silva et al., 2009). Our previous study found that hippocampal TERT is implicated in modulation of mood behaviors by regulation of proliferation of NPCs. The development of the newborn neurons contributes to the high synaptic plasticity and dynamic circuit incorporation of the DG, which plays a fundamental function in memory processing (Deng et al., 2010; Jaffe and Gutierrez, 2007; Nakashiba et al., 2012). However, the exact understanding of the molecular mechanism underlying the regulation of dendritic development and circuit formation of newborn neurons in the post-natal hippocampus is necessary (Ming and Song, 2011). Thus, in this study, we investigated the potential of hippocampal TERT in the modulation of neural development and its contribution to spatial

memory formation, as well as determining its cellular mechanism.

RESULTS

Hippocampal TERT Is Required for Spatial Memory Formation

It has been shown that TERT deficiency affects normal brain functions in mice (Yuan et al., 1999). To investigate whether TERT is implicated in hippocampus-dependent spatial memory formation, we performed the Morris water maze (MWM) test, a classic method for measuring spatial memory formation in rodents (D'Hooge and De Deyn, 2001), using the first generation of *Tert*$^{-/-}$ mice (Figure S1) and their wild-type (WT) mice. Surprisingly, *Tert*$^{-/-}$ mice displayed extremely poor ability in spatial learning and memory formation compared with WT in the MWM task (Figure 1A; Movies S1 and S2). To rule out the influence of swimming speed on platform probing, we monitored the swimming speed in each experiment. There was no difference in swimming speed between groups in each MWM task in this study (Table S1); and there was no difference in visible probe tests between groups in each MWM task (Figure S2).

In the adult brain, TERT is detected in various regions including the hippocampus (Caporaso et al., 2003). To determine whether TERT loss in the DG of *Tert*$^{-/-}$ mice accounts for the defect in spatial memory formation, we constructed a lentivirus (LV) expressing Flag-tagged mouse Tert full-length cDNA under control of the promoter, Ubi, and a GFP reporter gene under control of another promoter, SV40 (named LV-TERT-GFP; Figure 1B) to express the TERT protein and GFP separately. Western blot measurement showed that the TERT-Flag fusion protein was successfully detected by Flag primary antibody in cultured 293T cells 4 days after infection with LV-TERT-GFP (Figure 1B). Then, 1 μL of LV-TERT-GFP was microinjected into bilateral DGs of the hippocampi of *Tert*$^{-/-}$ mice (Figure 1C) to replenish TERT protein. As control, 1 μL of LV-GFP was microinjected into bilateral DGs of the hippocampi of *Tert*$^{-/-}$ and WT mice. Western blot measurement of Flag expression indicated that the TERT-Flag fusion protein was expressed in the DG of *Tert*$^{-/-}$ mice 14 days after injection of LV-TERT-GFP (Figure 1D). Strikingly, replenishment of TERT protein in the DG of *Tert*$^{-/-}$ mice significantly improved the ability of spatial learning and memory formation in the MWM task 30 days after infusion of LV-TERT-GFP (Figure 1E). In contrast, to specifically disrupt the expression of TERT protein in the DG, we delivered an LV vector expressing small hairpin RNA (shRNA) of TERT (LV-TERT-shRNA-GFP, Figure 1F) or LV-GFP into bilateral DGs. RT-PCR analysis showed 77.32% reduction of TERT mRNA expression level 7 days and 65.46% reduction 28 days after infusion of 1 μL of LV-TERT-shRNA-GFP into the DGs compared with 1 μL of LV-GFP infusion (Figure 1G). Importantly, an impaired ability in spatial memory formation in the MWM task of mice infused with LV-TERT-shRNA-GFP was observed 28 days after infusion, compared with mice infused with LV-GFP (Figure 1H), suggesting that specific TERT deficiency in the DG of the hippocampus impairs spatial memory formation. Altogether, these data suggest an essential role of hippocampal TERT in spatial memory formation.

High Level of Hippocampal TERT Facilitates Spatial Memory Formation

TERT overexpression in the hippocampus exerts an antidepressant effect (Zhou et al., 2011). To test whether overexpression of TERT in adult hippocampal DG promotes spatial memory formation, we delivered a recombinant adenoviral vector carrying the gene-encoding mouse TERT and GFP reporter cDNA linked by internal ribosome entry site (named AD-TERT-GFP) into the DGs by microinjection, and measured spatial memory formation in the MWM test 30 days after virus infection. TERT mRNA content measurement in the hippocampus showed that TERT expression was enhanced at day 7, peaked at day 14, began to decline at day 21, and returned to normal levels at day 28 after infusion of AD-TERT-GFP (Figure S3). Interestingly, AD-TERT-GFP infection in the DGs significantly improved spatial memory formation of mice in the MWM test 30 days (Figure 2A), but not 7 days (Figure 2B), after hippocampal microinjection. Taken together, these results imply that the positive impact of TERT overexpression on spatial memory formation is indirect, delayed, and requires a period of about 1 month.

TERT Is Essential for Dendritic Development *In Vitro* and in Adult DG

Neural development, especially of hippocampal newborn neurons in adulthood, is closely associated with memory formation (Bruel-Jungerman et al., 2007; Zhao et al., 2008). It is reported that telomere shortening caused by TERC knockout disrupts neuronal differentiation and neuritogenesis (Ferron et al., 2009). Although there is extensive evidence showing that telomere length is modulated by TERT, the role of TERT in neural development remains unknown. We accordingly speculated that TERT might be involved in spatial memory process via modulation of neural development, including adjusting morphological characteristics and sculpting the dendritic arbor.

To test this hypothesis, first, *in vitro* NSC differentiation experiments were performed using E18 embryonic hippocampus of *Tert*$^{-/-}$ and WT mice. Four days after induction of differentiation, analysis of doublecortin (DCX, a marker

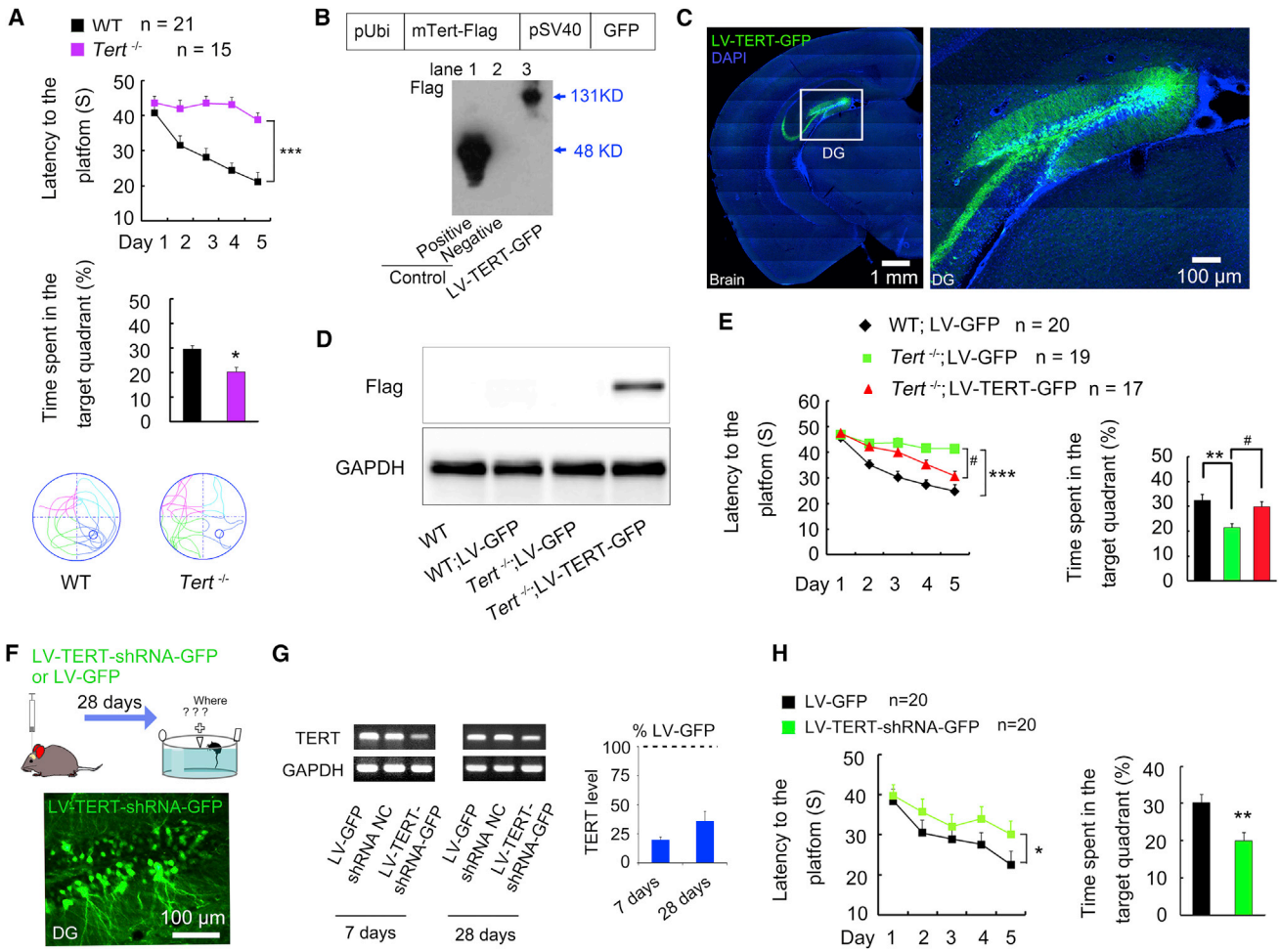

Figure 1. Loss of TERT in Adult DG Impairs Spatial Memory Formation

(A) Escape latency (upper, $F_{1,34} = 48.16$, ***p = 0.0001), time spent in target quadrant (middle, *p = 0.01) and representative swim paths (bottom) in MWM task. n = 15–21.

(B) Construction of LV-TERT-GFP. Western blot confirmed the expression of the TERT-Flag fusion protein in 293T cells. Lane 1: standard protein SURVIVIN-3Flag-GFP; lane 2: loading buffer; lane 3: 293T cells infected with LV-TERT-GFP. n = 3 independent experiments.

(C) Representative images showing the specific infection of LV-TERT-GFP in the DG.

(D) Western blot images of Flag and GAPDH 14 days after injection of LV-GFP or LV-TERT-GFP into the DG of *Tert*$^{-/-}$ or WT mice. n = 3 independent experiments.

(E) Re-expression of TERT by LV-TERT-GFP rescued the spatial memory defect in *Tert*$^{-/-}$ mice. Escape latency ($F_{2,55} = 19.87$, ***p = 0.0001, *Tert*$^{-/-}$:AD-GFP versus WT; AD-GFP; $^{\#}$p = 0.010, *Tert*$^{-/-}$:AD-TERT-GFP versus *Tert*$^{-/-}$:AD-GFP) (left) and time spent in target quadrant ($F_{2,55} = 7.9$, **p = 0.001, $^{\#}$p = 0.038) (right). n = 17–20.

(F and G) Representative RT-PCR (F) showing the mRNA level of TERT in the hippocampus of mice injected with LV-TERT-shRNA-GFP, LV-GFP, or shRNA negative control (shRNA NC) into the DG at days 7 and 28 after injection. n = 3 independent experiments. On the right, bar graph (G) showing the mRNA percentage level of TERT in mice that received LV-TERT-shRNA-GFP injection normalized to the LV-GFP group.

(H) Knockdown of TERT in the DG by shRNA resulted in spatial memory formation impairment. Escape latency (left, $F_{1,38} = 4.922$, *p = 0.0330), time spent in target quadrant (right, **p = 0.003). n = 20. Error bars, SEM. See also Figures S1 and S2, Table S1, and Movies S1 and S2.

for immature neurons) and glial fibrillary acid protein (GFAP, a marker for astrocytes) immunofluorescence signals showed that Tert knockout led to a reduction in neuronal fate as well as an increase in astrocytic fate (Figure 3A). Notably, the dendritic processes of 4-day-old DCX^{+} immature neurons from *Tert*$^{-/-}$ NSCs were significantly shorter than those from WT NSCs (Figure 3A). To confirm this phenomenon, second, we performed primary

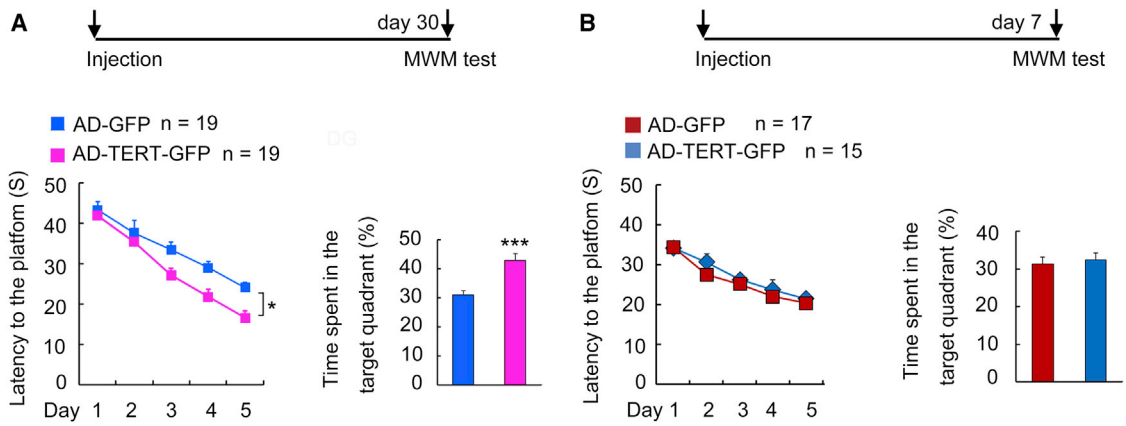

Figure 2. Increase of TERT in Adult DG Promotes Spatial Memory Formation

(A) Schedule designed. Escape latency ($F_{1,36}$ = 7.177, *p = 0.0110, left); time spent in target quadrant (***p = 0.0004, right). n = 19.
(B) Schedule designed. Escape latency ($F_{1,30}$ = 0.930, p = 0.4480, left); time spent in target quadrant (p = 0.6220, right). n = 15–17.
Error bars, SEM. See also Figure S3 and Table S1.

hippocampal neuronal culture from E18 embryonic hippocampus of *Tert*$^{-/-}$ and WT mice to compare the development of immature neurons. The data showed that Tert gene deletion led to a significant decrease in the total dendritic length and the number of branch points in 7-day-old DCX^{+} immature neurons cultured from the *Tert*$^{-/-}$ embryonic hippocampus, compared with 7-day-old neurons cultured from the WT embryonic hippocampus (Figure 3B). Third, in a primary hippocampal neuronal culture experiment, we infected the *Tert*$^{-/-}$ and WT NSCs at day 0 with AD-GFP for 24 hr. Morphology analysis of GFP^{+} mature neurons at day 14, when the cultured neurons became mature, also showed decreased total dendritic length and reduced number of branch points (Figure 3C), as well as diminished total spine and mushroom spine density (data not shown) in neurons cultured from the *Tert*$^{-/-}$ embryonic hippocampus compared with neurons cultured from the WT embryonic hippocampus. Taken together, these data uncover an important role for TERT in the morphological development of hippocampal neurons *in vitro*.

To know whether Tert knockout results in the impairment of neural development of granular neurons in adult DG, we performed Golgi staining on the brain sections of *Tert*$^{-/-}$ and WT mice. Consistent with the observation from the *in vitro* experiment, the Golgi-staining analysis showed relatively simple morphology of granular neurons and a significant reduction in total and mushroom spine density of granular neurons in the DG of *Tert*$^{-/-}$ mice compared with WT mice (Figure 4D). Anatomically, granular neurons in the DG send an output to neurons located in the CA3 to form the intrinsic "trisynaptic circuit" (DG→CA3→CA1) in the hippocampus (Neves et al., 2008). Synapsin I is present in the nerve terminal of axons and presents the synaptic contact (Sudhof et al., 1989). Synapsin I immunostaining showed lower levels of synapsin I expression in the intrinsic region of CA3 in *Tert*$^{-/-}$ mice compared with WT mice (Figure 4E). Western blot also showed significant decreased synapsin I expression in the hippocampus in *Tert*$^{-/-}$ mice compared with WT mice (Figure 4F). Thus, both the postsynaptic (spines detected by Golgi staining) and presynaptic (synapsin I immunostaining) evidence illustrated that TERT is essential for neural development in the hippocampus.

Adult-born neurons send afferent connectivity to CA3 neurons, contributing to the "trisynaptic circuit" and memory formation (Neves et al., 2008). To know whether the newborn neurons undergo abnormal development in the hippocampus of *Tert*$^{-/-}$ mice, we analyzed the morphology of DCX^{+} immature neurons in the adult DG (Figures 4G–4J). Remarkably, a reduction in total length and branching of dendrites of immature newborn neurons (Figures 4H–4J) was observed in the DG of the hippocampus of *Tert*$^{-/-}$ mice compared with WT mice. Therefore, these results demonstrate that TERT is also crucial for the development of newborn neurons in the adult hippocampus.

Elevated TERT Promotes Dendritic Development *In Vitro* and in Adult DG

Telomerase levels are high in stem/progenitor cells, neurons during early development, and decrease in association with cell differentiation. The TERT expression is undetectable in the vast majority of adult somatic cells. New neurons are differentiated from NSCs *in vitro* and NPCs in adult DG (Encinas et al., 2006). To directly and specifically overexpress TERT in the NSCs/NPCs, we constructed a recombinant retrovirus vector carrying full-length TERT cDNA and

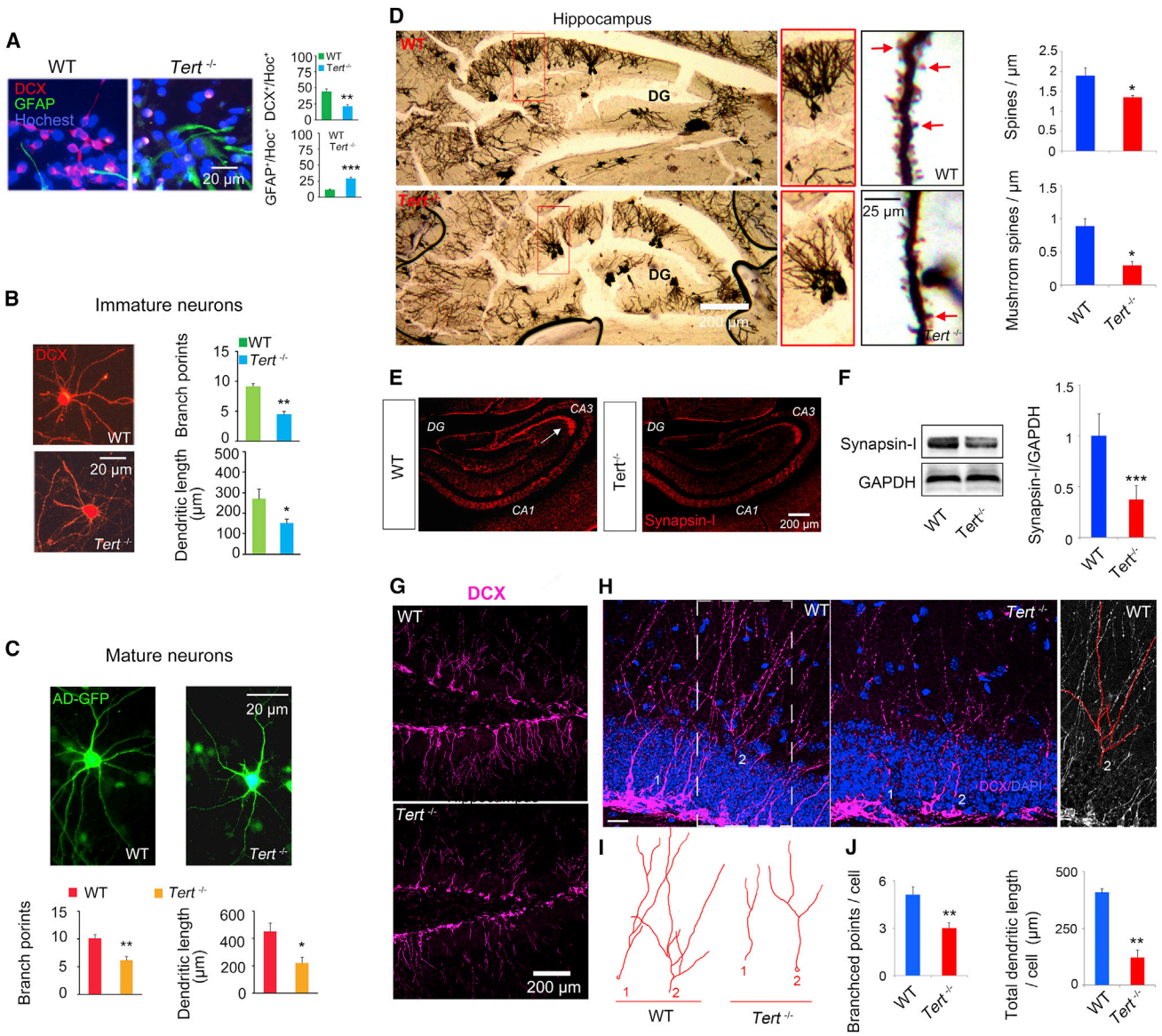

Figure 3. Tert Knockout Impairs Neural Development *In Vitro* and in Adult DG

(A) Representative images showing immunostaining with DCX and GFAP of cells at day 4 differentiated from *Tert*$^{-/-}$ and WT NSCs, and bar graph analysis. **p = 0.0088, ***p = 0.0008. n = 4 independent experiments.

(B) Representative images of DCX^{+} immature neurons from *Tert*$^{-/-}$ or WT mice at day 7 of primary hippocampal neuron culture. Bar graph showing the total dendritic branch number (n = 3 independent experiments, 4 neurons per sample, **p = 0.0023) and total dendritic length (n = 3 independent experiments, 4 neurons per sample, *p = 0.0159) per DCX^{+} neuron at day 7 of primary hippocampal neuron culture.

(C) Representative images of neurons at day 14 of primary hippocampal neurons cultured from *Tert*$^{-/-}$ or WT mice. Bar graph showing total dendritic branch number (n = 3 independent experiments, 4 neurons per sample, **p = 0.0042) and total dendritic length (n = 3 independent experiments, 4 neurons per sample, *p = 0.0196) per GFP^{+} neuron at day 14 of primary hippocampal neuron culture. Student's t test.

(D) Representative images of Golgi staining of the hippocampus showing the morphology of the granular neurons in the DG and the spines on the process. Red arrow indicates mushroom spine. Bar graph showing total spine density (n = 3 independent experiments, 12 neurons per sample, *p = 0.0441) and mushroom spine density (n = 3 independent experiments, 12 neurons per sample, *p = 0.0239) of granular cells in the hippocampal DG of *Tert*$^{-/-}$ or WT mice. Student's t test.

(legend continued on next page)

a GFP reporter gene under a CAG promoter to express a TERT-GFP fused protein (named RV-TERT-GFP, Figure S4), according to the ability of the retrovirus in infecting dividing cells. In primary hippocampal neuron culture, we treated the NSCs with RV-TERT-GFP or RV-GFP at day 0, and analyzed the morphology changes of the derived neurons at day 14. Despite the fact that the green fluorescence of RV-TERT-GFP-infected neurons was not as bright as that in RV-GFP-infected neurons, the morphology was well analyzed after synapsin I immunostaining (Figure 4A). The total dendritic length (Figure 4B) and the number of branch points (data not shown) were enhanced by RV-TERT-GFP. Meanwhile, analysis of synapsin I immunostaining showed that the synapsin I cluster density in the process significantly increased in RV-TERT-GFP-infected neurons compared with neurons infected with RV-GFP (Figure 4B). Moreover, increased synapsin I protein expression was detected in RV-TERT-GFP-infected neurons compared with RV-GFP-infected neurons by western blot (Figure 4C), indicating increased spine density and synapse formation induced by TERT overexpression in NSCs. However, the spine was not detectable because of the relative weak green fluorescence of GFP on the processes of RV-TERT-GFP infected neurons, possibly due to the fact that GFP was fused to the end of TERT. To directly explore the effect of TERT overexpression in NSCs on spine development, we then used LV-TERT-GFP and LV-GFP to infect cells to measure the spine density changes (Figures 4D and 4E). We infected the cells with LV-TERT-GFP or LV-GFP at day 0 for 24 hr during the 14-day primary neuron culture, and analyzed the morphology of the derived neurons at day 14. Both total spine and mushroom spine density of the cultured neurons significantly increased in LV-TERT-GFP$^+$ neurons compared with LV-GFP$^+$ neurons (Figures 4D and 4E). These data indicate that elevated TERT level in NSCs promotes neural development and neuritogenesis of the derived neurons *in vitro*.

Next, to verify the function of TERT in NPCs in adult DG, TERT was selectively overexpressed in dividing neural progenitors by delivering RV-TERT-GFP into the DG. Considering the weak GFP fluorescence of dendrites of the RV-TERT-GFP-infected neurons, we mixed RV-TERT-GFP with RV-red fluorescent protein (RFP), and then infused them together (1:1 ratio) into adult DG of WT mice. Twenty-eight days later, the morphology of the newborn neurons was examined by analyzing RFP fluorescence. In comparison with only RFP-positive neurons, which were only red without TERT overexpression, RV-RFP and RV-TERT-GFP double-infected neurons showed as yellow (a mixture of red and green) with TERT overexpression exhibited significantly enhanced length and branching of dendrites (Figures 4F and 4G), as well as spine and mushroom spine density (Figure 4H), demonstrating that elevated TERT in neural progenitors in adult DG promotes neural development and neuritogenesis *in vivo*.

Taken together, these data illustrate that TERT overexpression in NSCs/NPCs are beneficial for neural development, including morphological maturing and synaptic plasticity *in vitro* and in adult DG.

TERT Is Essential for Circuit Incorporation of Hippocampal Newborn Neurons

Hippocampal newborn neurons exhibit enhanced plasticity of integration into the existing network during maturation (Vivar et al., 2012). To identify the impact of TERT on the neuronal network formation of newborn neurons, we applied a monosynaptic retrograde tracing system based on retrovirus and pseudotyped rabies virus (Osakada and Callaway, 2013; Osakada et al., 2011; Vivar et al., 2012). A dose of 1 μL of retrovirus (RV-SYN-GTR) was injected into the right DG of *Tert*$^{-/-}$ and WT mice, followed by EnvA-pseudotyped rabies virus (EnvA-ΔR-mCh, 1 μL) injection into the same spot 1 month later (Figure 5A). The new developed neurons expressed nucleus-localized GFP, TVA receptor (T), and rabies glycoprotein (R) under control of the synapsin promoter 30 days after infection in NPCs. On day 30 after infection of EnvA-ΔR-mCh, in which Rgp gene of rabies was replaced with mCherry (mCh), EnvA-ΔR-mCh will enter TVA-expressing newborn neurons and produce rabies virus with Rgp to cross the synapse retrogradely (Figure 5A). All sections of mice brain were collected for analysis of starter cells (GFP$^+$ and mCherry$^+$) in the DG (Figure 5B) and traced cells (purely mCherry$^+$) throughout the brain 7 days later. To exclude that the

(E and F) Representative photos showing immunostaining with synapsin I in the hippocampus. The arrows indicate the reduced level of synapsin I in the CA3 of *Tert*$^{-/-}$ mice compared with WT mice (E). Representative images of western blot showing synapsin I in the hippocampus of *Tert*$^{-/-}$ or WT mice, and the bar graph analysis (***p = 0.0006) (F). Student's t test. n = 3 independent experiments.
(G–J) Representative images of immunostaining showing DCX$^+$ immature neurons in the DG of *Tert*$^{-/-}$ and WT mice (G). Analysis of the morphology of the DCX$^+$ immature neurons in the DG of *Tert*$^{-/-}$ and WT mice (H). Scale bar = 25 μm. Representative images of analyzed DCX$^+$ neurons in adult DG of *Tert*$^{-/-}$ and WT mice. The DCX$^+$ neurons with the most complicated morphology were chosen for analysis in each group (I). Bar graph showing total dendritic branch number (n = 3 independent experiments, 9 neurons per sample, **p = 0.0044) and total dendritic length (n = 3 independent experiments, 9 neurons per sample, **p = 0.0017) per DCX$^+$ neuron in the adult DG of *Tert*$^{-/-}$ or WT mice (J). Student's t test.
Error bars, SEM.

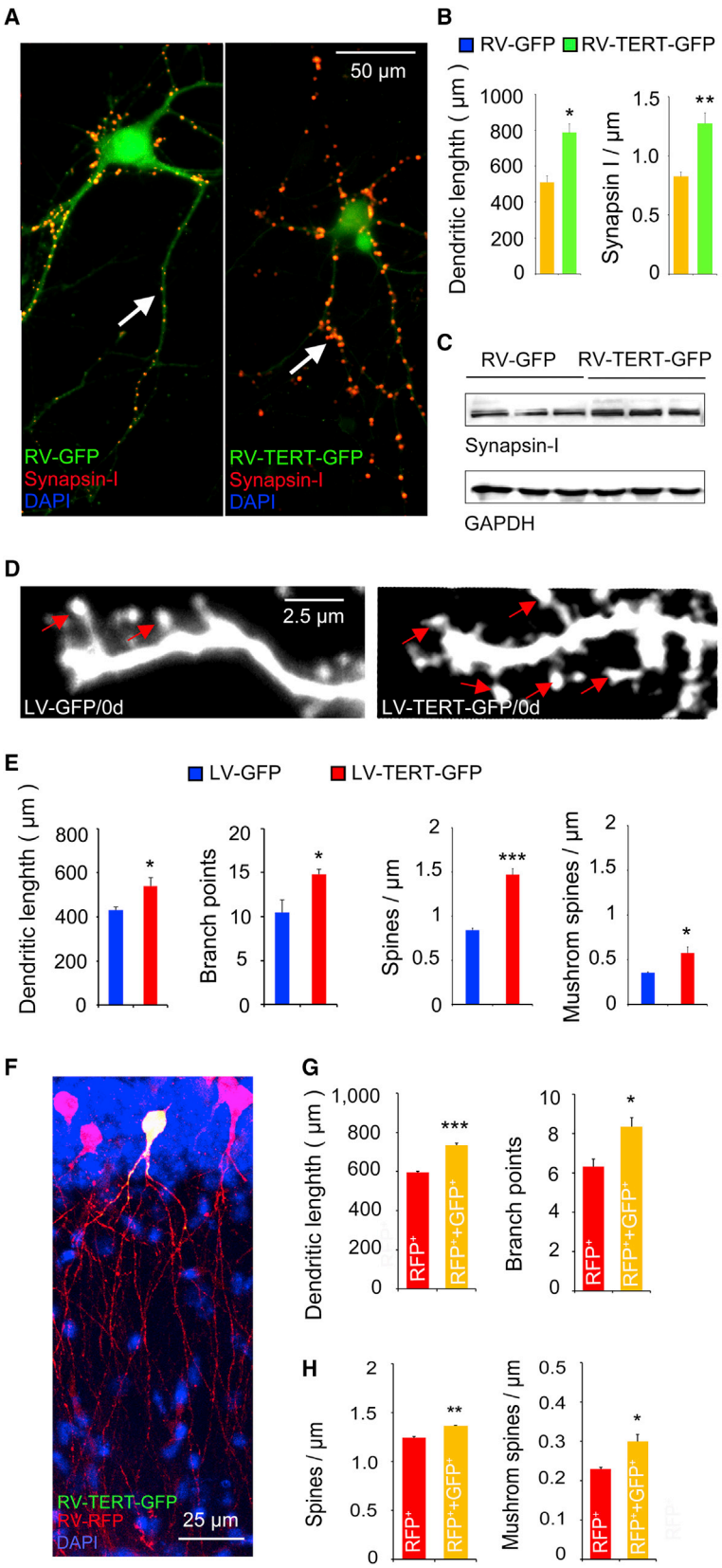

Figure 4. Overexpression of TERT Benefits Neural Development *In Vitro* and in Adult DG

(A–C) Representative images of primary cultured hippocampal neurons infected with RV-GFP or RV-TERT-GFP at day 1 for 24 hr showing the morphology at day 14 of culture. The arrows indicate the signal of synapsin I after synapsin I immunostaining (A). Bar graph showing total dendrite length (*p = 0.0106) and the density of synapsin I cluster (**p = 0.0098) 14 days after RV-GFP or RV-TERT-GFP infection in the primary hippocampal neuron culture. n = 8–10 neurons, Student's t test (B). Representative western blot photos showing the expression of synapsin I 14 days after RV-GFP or RV-TERT-GFP infection in the primary hippocampal neuron culture. n = 3 independent experiments. Student's t test (C).

(D and E) Representative images of spines on GFP$^+$ neurons at day 14 of primary hippocampal neuron culture. The NSCs were exposed to LV-TERT-GFP or LV-GFP at day 0 for 24 hr. Arrows indicate mushroom spines (D). Bar graph showing dendritic branch number (*p = 0.0102) and total dendritic length (*p = 0.0161), as well as spine (***p = 0.0009) and mushroom spine (*p = 0.0270) density, of neurons infected with LV-TERT-GFP or LV-GFP at day 0 for 24 hr. n = 10 neurons. Student's t test (E).

(F–H) A representative photo of newborn neurons infected with RV-TERT-GFP and RV-RFP in the DG 28 days after injection (F). The total dendritic length (***p = 0.0002) and branch points (*p = 0.0268) (G), and spine (**p = 0.0036) and mushroom spine (*p = 0.0168) density (H) of newborn neurons infected with RV-TERT-GFP and RV-RFP in the DG 28 days after injection. n = 3 independent experiments, Student's t test.

Error bars, SEM. See also Figure S4

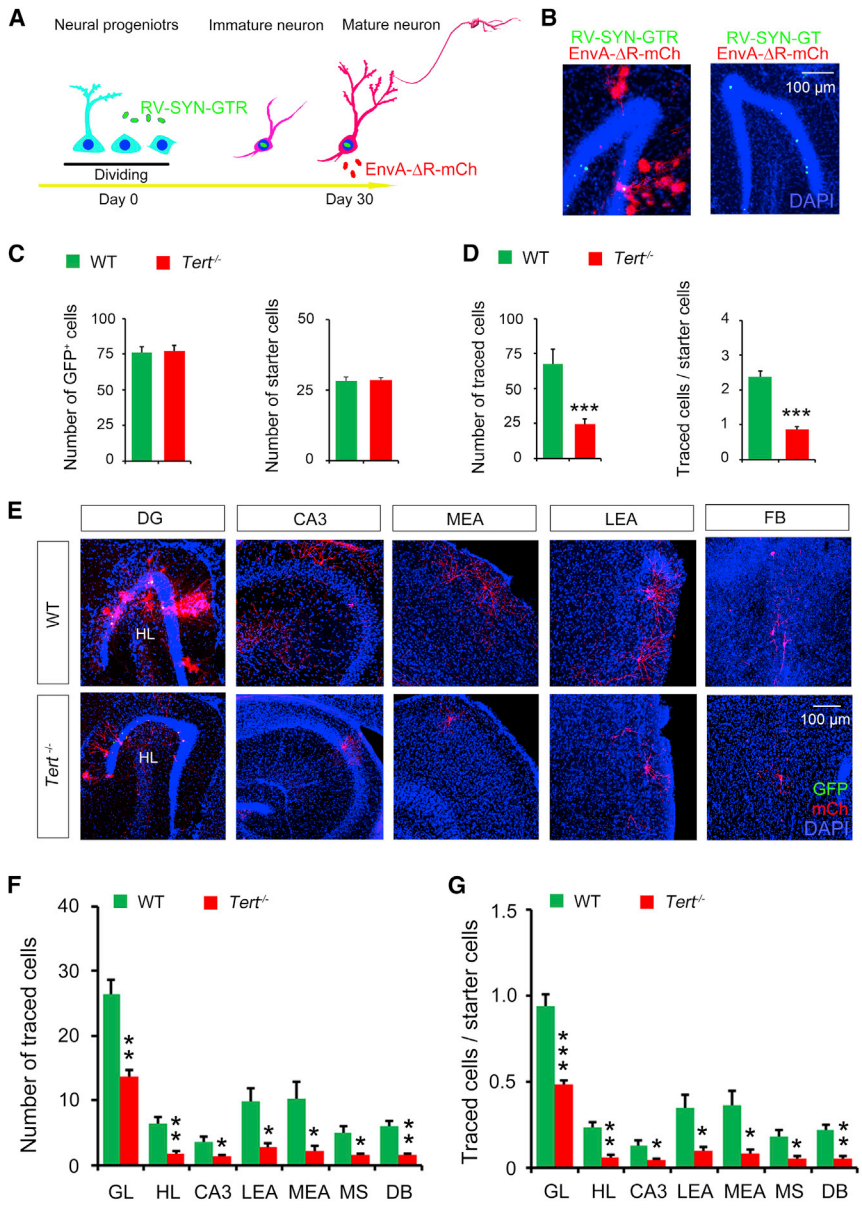

Figure 5. Deletion of TERT Gene Impairs Afferent Circuit Incorporation of Hippocampal Newborn Neurons

(A) A diagram showing the dual-virus retrograde tracing system used to trace afferent cells of hippocampal newborn neurons.

(B) Representative photos showing the GFP$^+$ cells, starter cells, and traced cells in the DG after injection of RV-SYN-GTR and EnvA-ΔG-mCh (left). As control, RV-SYN-GT lacking rabies glycoprotein was injected 30 days before EnvA-ΔG-mCh injection. No starter cells or traced cells were observed in this situation.

(C and D) Bar graphs showing the number of GFP$^+$ cells and starter cells in the DG of *Tert*$^{-/-}$ or WT mice. $n = 4$, Student's t test (C). Bar graphs showing the number of traced cells (***p = 0.0004) and the ratio of traced cells/starter cells (***p = 0.0001) in *Tert*$^{-/-}$ or WT mice. n = 4 independent experiments, Student's t test (D).

(E–G) Representative images showing the distribution of input cells throughout the brain (E). Bar graphs showing the number of traced cells (F) and the ratio of traced cells/starter cells (G) in regions of the brain. n = 4 independent experiments, Student's t test for each region. *p < 0.05, **p < 0.01, ***p < 0.001. DG, dentate gyrus; HL, hilus; MEA, medial entorhinal area; LEA, lateral entorhinal area; MS, medial septum; DB, diagonal band.

Error bars, SEM.

EnvA-ΔR-mCh was not successfully pseudotyped, RV-SYN-GT without rabies glycoprotein codons was injected into the DG, followed by EnvA-ΔR-mCh injection 1 month later, and no traced cell was detected in the whole brain, validating the specificity of this tracing system (Figure 5B).

Previously, we found that inhibition of TERT activity reduced the proliferation of NPCs in the DG (Zhou et al., 2011), so we infused a titer of ~1 × 107 pfu/mL of RV-SYN-GTR into the right DG of WT mice and a titer of ~2 × 107 pfu/mL of RV-SYN-GTR into the right DG of *Tert*$^{-/-}$ mice. Accordingly, the number of pure GFP$^+$ cells and starter cells were almost identical between *Tert*$^{-/-}$ and WT mice (Figure 5C). However, the total number of traced cells and the ratio of traced cells per single newborn neuron were significantly lower in *Tert*$^{-/-}$ mice compared with WT mice (Figure 5D). One-month-old newborn neurons receive afferent inputs from the intra-hippocampus, including the granular layer, the hilus, and CA3, the entorhinal cortex, including the lateral and medial entorhinal areas, and the forebrain, including the medial septum and diagonal band (Figure 5E). Interestingly, TERT deficiency resulted in reduced afferent input globally throughout the brain (Figures 5E and 5F). Moreover, the input onto single new neuron was remarkably lessened in *Tert*$^{-/-}$ mice compared with WT mice (Figure 5G). These data suggest that the incorporation of hippocampal

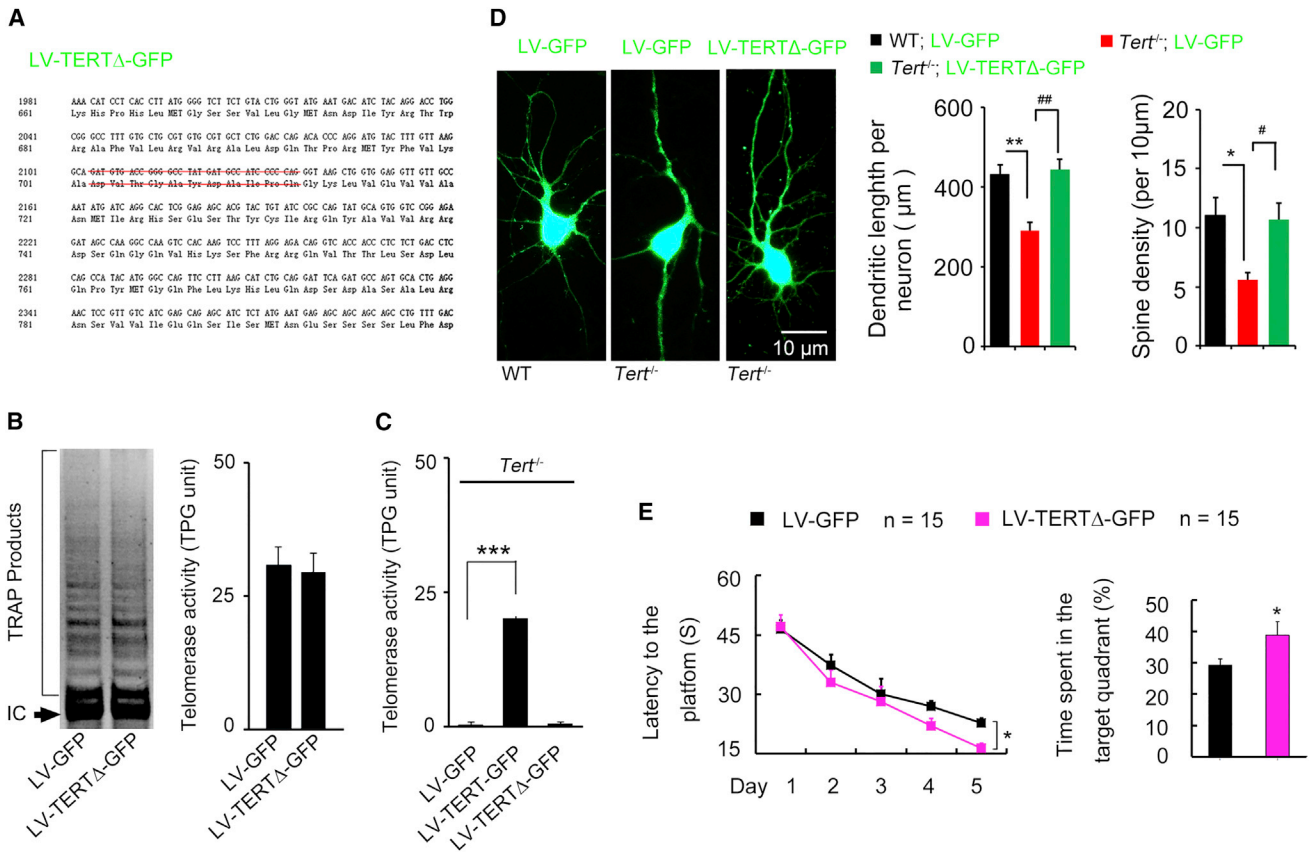

Figure 6. Catalytic Activity of TERT Is Not Required for Modulation of Neural Development and Spatial Memory Formation

(A) The design of construction of a lentiviral vector expressing a type of catalytically inactive TERT.

(B and C) Representative TRAP image (left) and bar graph (right) showing telomerase activity in the adult DG infected with LV-TERTΔ-GFP or LV-GFP 7 days after infection (n = 3 independent experiments, p = 0.8165, Student's t test), (B). Bar graph showing telomerase activity in the adult DG of *Tert*$^{-/-}$ mice infected with LV-GFP, LV-TERT-GFP or LV-TERTΔ-GFP 14 days after injection (n = 3 independent experiments, $F_{2,6}$ = 48.58, ***p = 0.0002, one-way ANOVA), (C).

(D) Representative images of primary cultured hippocampal neurons from *Tert*$^{-/-}$ or WT mice. The cells were infected with LV-GFP or LV-TERTΔ-GFP at day 0 of culture. Bar graph showing total dendritic length ($F_{2,12}$ = 12.89, **p = 0.0010, $^{\#\#}$p = 0.0018) and spine density ($F_{2,12}$ = 5.961, *p = 0.0159, $^{\#}$p = 0.0351) per GFP^{+} neuron at day 14 of primary hippocampal neuron culture. n = 5 independent experiments, one-way ANOVA.

(E) Escape latency measured during days 30–34 ($F_{1,28}$ = 4.346, *p = 0.041) and time spent in target quadrant (*p = 0.019) measured at day 35 after microinjection of LV-TERTΔ-GFP or LV-GFP into the adult DGs of mice in MWM task. n = 15.

Error bars, SEM. See also Figure S7 and Table S1

newborn neurons into the existing brain circuits is impaired in the brain lacking the *Tert* gene, implying an important role for TERT in neural circuit formation.

TERT Regulates the Dendritic Development Independently of Telomerase Activity

The catalytic activity-independent function of TERT has been reported (Sarin et al., 2005). To determine whether the telomerase activity of TERT is required in the modulation of neural development, we constructed recombinant LV carrying non-activity TERT cDNA (LV-TERTΔ-GFP), in which the nucleotides encoding the key amino acids (AA702–712) for maintaining the catalytic activity were deleted (Figure 6A). TRAP measurement showed that infection of LV-TERTΔ-GFP in the DG did not increase telomerase activity compared with LV-GFP infection, indicating that the shortened TERT (TERTΔ) lacked catalytic activity (Figure 6B). Furthermore, TRAP analysis of telomerase activity in the DG of the hippocampus of *Tert*$^{-/-}$ mice infected with LV-GFP, LV-TERT-GFP, or LV-TERTΔ-GFP showed that LV-TERT-GFP, but not LV-TERTΔ-GFP infection rescued telomerase activity loss induced by Tert knockout (Figure 6C). However, in a primary hippocampal neuronal culture experiment, similar to LV-TERT-GFP

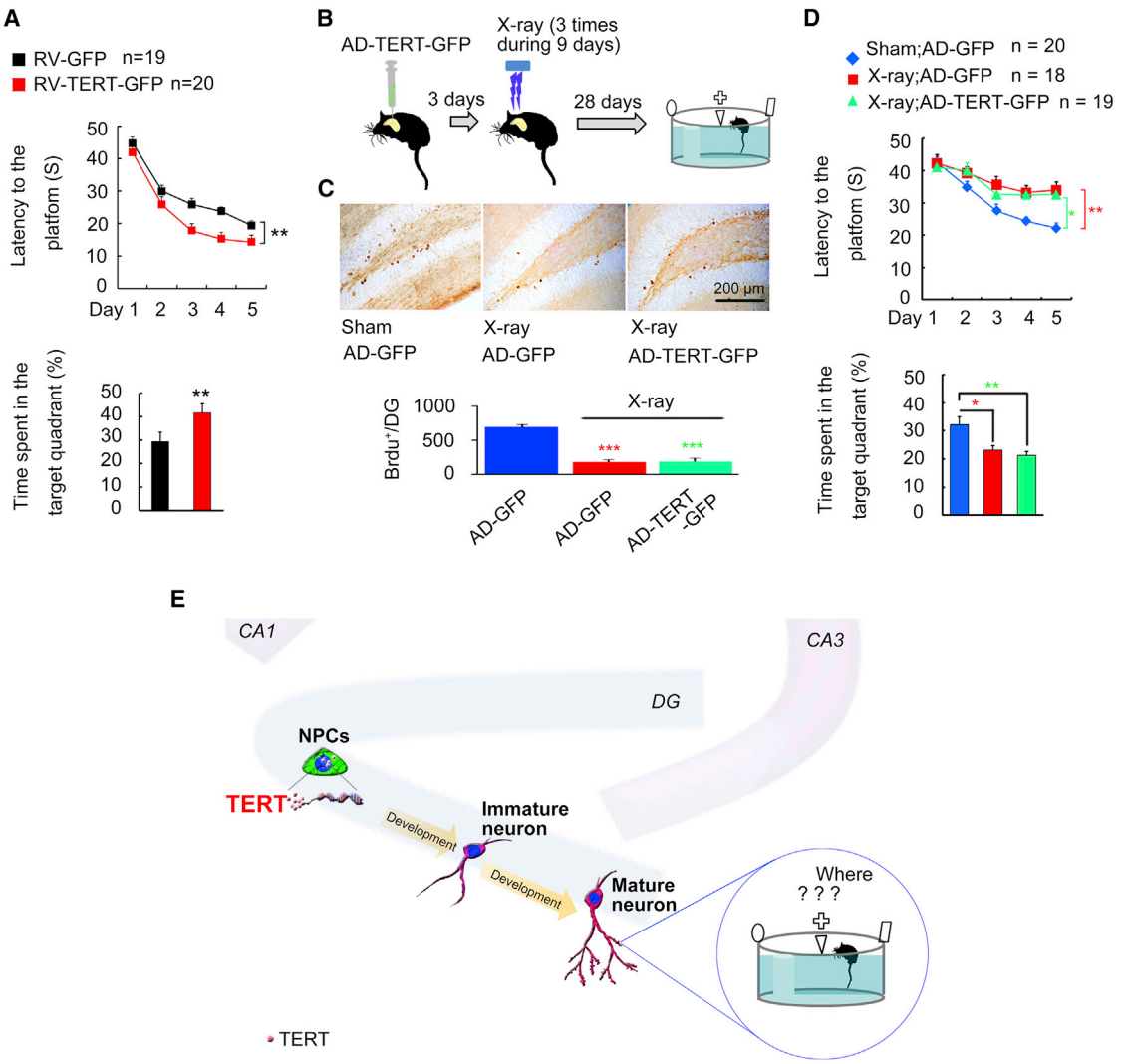

Figure 7. The Regulation of Spatial Memory by TERT Requires Newborn Neurons

(A) Escape latency ($F_{1,37}$ = 10.86, **p = 0.0020) and time spent in the target quadrant (**p = 0.0080, Student's t test) in MWM test. n = 19–20.

(B–D) Schematic representation of the experiment. BrdU was administered during days 8–10 after AD infection (B). Representatives of the $BrdU^+$ cells in the DG. Scale bars, = 200 μm. Total number of BrdU + cells per DG at day 28 after BrdU labeling (n = 4 independent experiments, $F_{2,9}$ = 59.24, ***p < 0.0001, versus sham; AD-GFP, one-way ANOVA), (C). X-ray irradiation of the hippocampus zone blocked AD-TERT-GFP-induced improvement of spatial memory formation in the MWM task. Escape latency measured during days 41–45 ($F_{2,54}$ = 6.354, **p = 0.0030, sham; AD-GFP versus X-ray; AD-GFP; *p = 0.0490, sham; AD-GFP versus X-ray; AD-TERT-GFP) and time spent in target quadrant measured at day 46 ($F_{2,54}$ = 6.620, *p = 0.025, **p = 0.005, versus sham; AD-GFP, one-way ANOVA), (D). n = 18–20.

(E) A model showing that TERT in NPCs in the DG of adult hippocampus regulates spatial memory formation by modulation of the development of newborn neurons.

Error bars, SEM. See also Figures S5 and S7; Table S1.

(Figures 4D and 4E), replenishing non-activity TERT (TERTΔ) in $Tert^{-/-}$ NSCs by LV-TERTΔ-GFP also rescued the reduction in total dendritic length and spine density of the $Tert^{-/-}$ NSC-derived neurons (Figure 6D), indicating an dispensable role of TERT catalytic activity in the modulation of neural development. To test whether non-activity TERT expression in the DG would enhance the ability of spatial memory formation, we delivered LV-TERTΔ-GFP or LV-GFP into the DG of WT mice. The MWM task was performed 28 days after infusion and showed that expression of shortened TERT without catalytic activity in the DG also facilitated spatial memory formation (Figure 6E). These

data demonstrate that the function of TERT in the regulation of neural development and spatial memory formation does not require the telomerase non-canonical activity.

Hippocampal Newborn Neurons Account for the Function of TERT in Processing Spatial Memory

Although the spatial memory formation in both *Tert*$^{-/-}$ and WT mice was enhanced by virus-mediated TERT overexpression in the DG (Figures 1 and 2), it remained unclear which type of cells mediated this effect. Histological analyses of the expression of cell type-specific markers in GFP-expressing cells revealed that LV-TERT-GFP/LV-GFP infected NeuN^{+} neurons, GFAP^{+} astrocytes, and SOX2^{+}/Ki67^{+} neural progenitors in the DG (Figure S5). Adult-born neurons in the DG contribute to the formation of new memories, particularly spatial memory (Zhao et al., 2008). It takes about 4 weeks for newborn neurons proliferated from NPCs in the DG to mature and to play a role in spatial memory processes (Lledo et al., 2006; Zhao et al., 2008). The effect of LV-TERT-GFP and AD-TERT-GFP on spatial memory formation appeared 28 days after infection (Figures 1E and 2), which was exactly the same time required for maturation of newborn neurons. Thus, we speculated that NPC-generated adult-born neurons account for the memory improvement by TERT. To verify this hypothesis, TERT was specifically overexpressed in proliferating NPCs by injection of RV-TERT-GFP at high titers into the DGs and measured the spatial memory formation 28 days later. As expected, overexpression of TERT in dividing neural progenitors in the DG was sufficient to induce spatial memory improvement (Figure 7A).

X-ray irradiation is developed to ablate neurogenesis and investigate the function of newborn neurons in the hippocampus (Santarelli et al., 2003). We used X-ray irradiation to estimate the role of hippocampal newborn neurons in the TERT-induced enhancement of spatial memory formation. We killed proliferating NPCs by selectively exposing the bilateral hippocampus zone to X-ray irradiation 3 days after hippocampal injection of AD-TERT-GFP (5 Gy each time, at days 4, 7, and 10; Figure 7B). Then, bromodeoxyuridine (BrdU) (50 mg/kg, intraperitoneally [i.p.] 2 times per day) was administrated in mice at days 8–10. Cell damage was examined by staining the brain slices with Fluoro-Jade (FJ) which is used as fluorescent markers for neuronal death (Luo et al., 2007). Twenty-four hours after the end of the last X-ray irradiation, mice were killed to perform FJ staining. It was shown that irradiation caused a marked increase in the number of FJ-positive cells, predominantly confined to the sub-granular layer (Figure S6). Meanwhile, intraluminal middle cerebral artery occlusion (MCAO)-induced ischemia mice brain was used as positive control and a lot of FJ-positive cells were found in the DG and CA1 24 hr after MCAO surgery (Figure S6). BrdU immunostaining analysis, 28 days later, confirmed that the newborn neurons were killed by X-ray irradiation in both AD-GFP- and AD-TERT-GFP-infected DG mice, compared with the sham mice (Figure 7C). No difference in the number of BrdU^{+} newborn cells was found between AD-GFP- and AD-TERT-GFP-injected DG (Figure 7C). As a result, in comparison with X-ray irradiaton, in AD-GFP-injected mice, TERT overexpression-induced improvement of spatial memory formation was blocked by irradiation 28 days later (Figure 7D), suggesting that hippocampal newborn neurons mediate the regulation of spatial memory formation by hippocampal TERT (Figure 7E). Hence, TERT in the NPCs in the DG of the hippocampus is an important endogenous factor for spatial memory formation through influencing the development, neuritogenesis, and circuit incorporation of hippocampal newborn neurons.

DISCUSSION

The function of telomerase in adult tissue beyond cellular aging, proliferation, and turnover remains unexplored (Jaskelioff et al., 2011; Montgomery et al., 2011; Sahin and Depinho, 2010; Zhou et al., 2011). In particular, the function of telomerase in the DG of adult hippocampus is largely unknown. Our study uncovered an unknown role for hippocampal TERT, the catalytic subunit of telomerase, in the dendritic development, neuritogenesis, and circuit incorporation of newborn neurons as well as in spatial memory processing. Of note, the function of TERT in NPCs in modulation of neural development is not telomerase activity dependent, implying that TERT designed to be without catalytic activity could be used for improving memory formation without tumorigenesis. Our finding would be helpful for understanding the molecular mechanism of spatial memory formation and would represent a potential target for a treatment approach for injury-related memory disorders.

TERC, another subunit of telomerase, is found to be required for the neuritogenesis of neurons by using late-generation Terc knockout mice. Compared with humans, mice possess much longer telomeres at the end of chromosomes. Hence, the impaired neural development in G4 *Terc*$^{-/-}$ mice is the consequence of shortening telomere in NSCs (Ferron et al., 2009). TERT catalytic function also serves for telomere elongation. More surprisingly, here, we found that TERT modulates neural development via a very different mechanism. In the first generation of *Tert*$^{-/-}$ mice, the dendritic development, neuritogenesis, and circuit incorporation of hippocampal newborn neurons were disrupted. In addition, TERT shRNA interference and overexpression by viral vehicles affected neural

development. These data demonstrated that telomere shortening is not important in the action of TERT in modulation of neural development. Indeed, by generating an edited version of TERT without catalytic activity, a non-activity-dependent role of TERT was revealed in the regulation of neural development and spatial memory formation.

Our previous study found that hippocampal TERT is involved in depression-related behavior (Zhou et al., 2011). It is possible that the activity of mice in MWM tests after TERT alteration is influenced by, or the direct consequence of, the depression-related behavior phenotype. To investigate this, we measured the depression-related behavior tests, including the tail suspension test and the forced swimming test (FST) 28 days after injection of LV-TERTΔ-GFP and LV-GFP into the DG of WT mice (Figure S7). Although, spatial memory formation was enhanced by LV-TERTΔ-GFP (Figure 6), depression-related behavior was not observed (Figure S7). Thus, the behavior alteration in the MWM test after TERT manipulation may not be associated with depressive mood changes. There is extensive evidence showing that hippocampal neurogenesis contributes to memory formation in normal physical states and in disease states such as aging, Alzheimer's disease, and dementia (Squire, 1992a). Our previous study demonstrates that TERT regulates hippocampal neurogenesis (Zhou et al., 2011). Therefore, hippocampal TERT could modulate spatial memory formation by adjusting both the number of newborn neurons and the morphological complexity of the newly developed neurons.

TERT is demonstrated to have a strong correlation with tumorigenesis and a causal relevance with lifespan and aging, since there are high levels of TERT in cancer stem cells and embryonic stem cells (Harley, 2008; Jaskelioff et al., 2011). Meanwhile, TERT is also highly expressed in NSCs/NPCs (Zhou et al., 2011). Besides its important role in proliferation, the exact role for TERT in the NSCs/NPCs is unclear. By using *Tert* knockout mice and viral tools, we demonstrated an important role of TERT in neural development including dendritic development, neuritogenesis, and circuit incorporation. The question is: how does TERT in the NSCs/NPCs affect the development of the newborn neurons? The molecule β-catenin is an important signaling molecule mediating the gene transcription of the Wnt pathway. Both Wnt and β-catenin were found to be involved in the development of newborn neurons in the DG (Budnik and Salinas, 2011; Gao et al., 2007). Previous research shows that β-catenin binds to the TERT promoter for the regulation of TERT expression (Hoffmeyer et al., 2012). Moreover, it is found that TERT modulates Wnt/β-catenin signaling by association with the target gene chromatin (Park et al., 2009). Hence, TERT may interact with the Wnt/β-catenin cascade in regulating dendritic development of the post-natal-born neurons.

Upon joining DG circuits, the newly born neurons in adult DG are more likely to be recruited into emerging memory traces (Deng et al., 2010). In particular, the development of the newborn neurons is critical for the neuroplasticity and the function of the hippocampus, including memory formation under physiological conditions (Bruel-Jungerman et al., 2007) or in disease states such as aging, Alzheimer's disease, or dementia (Squire, 1992a). Our tracing data showed that the input circuit establishment of hippocampal newborn neurons was reduced in Tert knockout mice compared with WT mice. Because *Tert* knockout may affect neural development globally, the impaired development of the afferent neurons may also contribute to this observation. Although this data imply that TERT is important for neural circuits formation, further selective manipulation of TERT in the "starter" newborn neurons in the tracing system could be helpful to understand the direct function of TERT in PNCs in the modulation of the circuitry of hippocampal newborn neuron.

Based on our finding here, a type of none-activity TERT strategy could be adopted for gene therapy to improve memory, providing a potential target for NSCs-based treatment of aging-caused impairment of memory formation.

EXPERIMENTAL PROCEDURES

For a more detailed description, see Supplemental Experimental Procedures.

Animals

Young adult (7- to 8-week-old) male ICR or FVB/NJU mice were used in this study. $Tert^{-/-}$ mice (1.5–2.5 months old) used in this study were produced by intercrosses of homozygous knockout mice (Yuan et al., 1999) that were backcrossed to FVB/NJU mice over more than ten generations. Then, the first generation of $Tert^{-/-}$ mice was used for analysis in this study. Animals were housed in an air-conditioned room (20 ± 2°C), with food and water *ad libitum*, except when specified otherwise. All procedures involving the use of animals were approved by the Institutional Animal Care and Use Committee of Nanjing Medical University (protocol number: IACUC-1704010). All experiments were performed in accordance with the approved guidelines and regulations.

The MWM Test

The MWM test was performed as described with a few adjustments (Li et al., 2009). The training paradigm for the visible platform version of the MWM consisted of four trials (60 s maximum; 15 min interval) each day for 2 consecutive days. Following visible platform training, the training paradigm for the hidden platform version of the MWM consisted of four trials (60 s maximum; 15 min interval) each day for 5 consecutive days. The probe trial was carried out 24 hr after the completion of training on day 6. The swim paths were recorded with a video tracking system

(EthoVision XT). The data of the mice which were floating or jumping off the platform in the MWM test was excluded.

Golgi Staining

Brains were cut to cross-sections 200 μm thick with a Vibratome (Leica) and stained with Golgi dye (Guan et al., 2009). Sections were analyzed with a Zeiss Axiovert 200M microscope and Openlab software. The number of apical and basal spines on hippocampal DG neurons was counted blind to the genotype. Images of neurons stained with Golgi dye were acquired with the Olympus phase contrast microscope with a 40× oil lens. The image files were used for analysis with the Imaris v.7.2.3 program. For each experimental group, a minimum of 4 cells per slice (4 slices per mouse, totally 12 neurons per mouse) were analyzed. The type of spines was identified based on the shape and width of spines. When the width value was >0.6 μm, the spines were classified as mushroom spines.

Statistics

Statistical analysis for escape latency in the MWM test: repeated measures ANOVA followed by a *post hoc* Bonferroni multiple comparison tests. Statistical analysis for probe test: Student's t test (two groups) or one-way ANOVA (three groups). All graphical data were presented as means ± SEM.

SUPPLEMENTAL INFORMATION

Supplemental Information includes Supplemental Experimental Procedures, seven figures, one table, and two movies and can be found with this article online at http://dx.doi.org/10.1016/j.stemcr.2017.06.014.

AUTHOR CONTRIBUTIONS

D.Y.Z. and Q.G.Z. designed and guided the research; Q.G.Z., M.Y.L., H.Y.W., H.Z., X.R.S., and X.L. performed the research. F.I., H.W.L., and S.D. provided *Tert*$^{-/-}$ mice and the genotyping strategy. Q.G.Z., Z.G.L., and H.S. constructed the virus. Xin Jin helped with culture of adult NSCs. H.H.Z., J.Z., Y.Z., Xun Jin, E.J.R., and Y.H.L. supported technology. Q.G.Z. and M.Y.L. analyzed data. Q.G.Z., D.Y.Z., and H.S. wrote the manuscript.

ACKNOWLEDGMENTS

We thank Edward Callaway of the Salk Institute for Biological Studies for providing the pseudotyped rabies virus construction system. The authors would like to thank Chun-Xia Luo and Lei Chang for cell culture advice. This work was supported by grants from the National Natural Science Foundation of China (91232304, 31530091, 81370033, 81571269, 81572891), the National Key Research and Development Program of China (2016YFC1306703), and the Natural Science Foundation of Jiangsu Province (BK2011029, BK20140964, BK20140366), by the Key Lab of Cardiovascular and Cerebrovascular Drugs of Jiangsu Province, and by the Collaborative Innovation Center For Cardiovascular Disease Translational Medicine for data collection, analysis, and interpretation. This study was also supported by the National Institute on Alcohol Abuse and Alcoholism (R01AA022377), the Whitehall Foundation (to H.S), and the American Federation for Aging Research (to H.S.)

Received: March 20, 2017
Revised: June 27, 2017
Accepted: June 27, 2017
Published: July 27, 2017

REFERENCES

Ayala, R., Shu, T., and Tsai, L.H. (2007). Trekking across the brain: the journey of neuronal migration. Cell *128*, 29–43.

Blackburn, E.H. (2001). Switching and signaling at the telomere. Cell *106*, 661–673.

Bruel-Jungerman, E., Rampon, C., and Laroche, S. (2007). Adult hippocampal neurogenesis, synaptic plasticity and memory: facts and hypotheses. Rev. Neurosci. *18*, 93–114.

Budnik, V., and Salinas, P.C. (2011). Wnt signaling during synaptic development and plasticity. Curr. Opin. Neurobiol. *21*, 151–159.

Cai, J., Wu, Y., Mirua, T., Pierce, J.L., Lucero, M.T., Albertine, K.H., Spangrude, G.J., and Rao, M.S. (2002). Properties of a fetal multipotent neural stem cell (NEP cell). Dev. Biol. *251*, 221–240.

Caporaso, G.L., Lim, D.A., Alvarez-Buylla, A., and Chao, M.V. (2003). Telomerase activity in the subventricular zone of adult mice. Mol. Cell. Neurosci. *23*, 693–702.

D'Hooge, R., and De Deyn, P.P. (2001). Applications of the Morris water maze in the study of learning and memory. Brain Res. Brain Res. Rev. *36*, 60–90.

Deng, W., Aimone, J.B., and Gage, F.H. (2010). New neurons and new memories: how does adult hippocampal neurogenesis affect learning and memory? Nat. Rev. Neurosci. *11*, 339–350.

Encinas, J.M., Vaahtokari, A., and Enikolopov, G. (2006). Fluoxetine targets early progenitor cells in the adult brain. Proc. Natl. Acad. Sci. USA *103*, 8233–8238.

Ferron, S., Mira, H., Franco, S., Cano-Jaimez, M., Bellmunt, E., Ramirez, C., Farinas, I., and Blasco, M.A. (2004). Telomere shortening and chromosomal instability abrogates proliferation of adult but not embryonic neural stem cells. Development *131*, 4059–4070.

Ferron, S.R., Marques-Torrejon, M.A., Mira, H., Flores, I., Taylor, K., Blasco, M.A., and Farinas, I. (2009). Telomere shortening in neural stem cells disrupts neuronal differentiation and neuritogenesis. J. Neurosci. *29*, 14394–14407.

Gao, X., Arlotta, P., Macklis, J.D., and Chen, J. (2007). Conditional knock-out of beta-catenin in postnatal-born dentate gyrus granule neurons results in dendritic malformation. J. Neurosci. *27*, 14317–14325.

Guan, J.S., Haggarty, S.J., Giacometti, E., Dannenberg, J.H., Joseph, N., Gao, J., Nieland, T.J., Zhou, Y., Wang, X., Mazitschek, R., et al. (2009). HDAC2 negatively regulates memory formation and synaptic plasticity. Nature *459*, 55–60.

Harley, C.B. (2008). Telomerase and cancer therapeutics. Nat. Rev. Cancer *8*, 167–179.

Hoffmeyer, K., Raggioli, A., Rudloff, S., Anton, R., Hierholzer, A., Del Valle, I., Hein, K., Vogt, R., and Kemler, R. (2012). Wnt/beta-catenin signaling regulates telomerase in stem cells and cancer cells. Science *336*, 1549–1554.

Jaffe, D.B., and Gutierrez, R. (2007). Mossy fiber synaptic transmission: communication from the dentate gyrus to area CA3. Prog. Brain Res. *163*, 109–132.

Jaskelioff, M., Muller, F.L., Paik, J.H., Thomas, E., Jiang, S., Adams, A.C., Sahin, E., Kost-Alimova, M., Protopopov, A., Cadinanos, J., et al. (2011). Telomerase reactivation reverses tissue degeneration in aged telomerase-deficient mice. Nature *469*, 102–106.

Li, W.L., Cai, H.H., Wang, B., Chen, L., Zhou, Q.G., Luo, C.X., Liu, N., Ding, X.S., and Zhu, D.Y. (2009). Chronic fluoxetine treatment improves ischemia-induced spatial cognitive deficits through increasing hippocampal neurogenesis after stroke. J. Neurosci. Res. *87*, 112–122.

Lledo, P.M., Alonso, M., and Grubb, M.S. (2006). Adult neurogenesis and functional plasticity in neuronal circuits. Nat. Rev. Neurosci. *7*, 179–193.

Luo, C.X., Zhu, X.J., Zhou, Q.G., Wang, B., Wang, W., Cai, H.H., Sun, Y.J., Hu, M., Jiang, J., Hua, Y., et al. (2007). Reduced neuronal nitric oxide synthase is involved in ischemia-induced hippocampal neurogenesis by up-regulating inducible nitric oxide synthase expression. J. Neurochem. *103*, 1872–1882.

Ming, G.L., and Song, H. (2011). Adult neurogenesis in the mammalian brain: significant answers and significant questions. Neuron *70*, 687–702.

Montgomery, R.K., Carlone, D.L., Richmond, C.A., Farilla, L., Kranendonk, M.E., Henderson, D.E., Baffour-Awuah, N.Y., Ambruzs, D.M., Fogli, L.K., Algra, S., et al. (2011). Mouse telomerase reverse transcriptase (mTert) expression marks slowly cycling intestinal stem cells. Proc. Natl. Acad. Sci. USA *108*, 179–184.

Nakashiba, T., Cushman, J.D., Pelkey, K.A., Renaudineau, S., Buhl, D.L., McHugh, T.J., Rodriguez Barrera, V., Chittajallu, R., Iwamoto, K.S., McBain, C.J., et al. (2012). Young dentate granule cells mediate pattern separation, whereas old granule cells facilitate pattern completion. Cell *149*, 188–201.

Nandakumar, J., and Cech, T.R. (2013). Finding the end: recruitment of telomerase to telomeres. Nat. Rev. Mol. Cell Biol. *14*, 69–82.

Neves, G., Cooke, S.F., and Bliss, T.V. (2008). Synaptic plasticity, memory and the hippocampus: a neural network approach to causality. Nat. Rev. Neurosci. *9*, 65–75.

Osakada, F., and Callaway, E.M. (2013). Design and generation of recombinant rabies virus vectors. Nat. Protoc. *8*, 1583–1601.

Osakada, F., Mori, T., Cetin, A.H., Marshel, J.H., Virgen, B., and Callaway, E.M. (2011). New rabies virus variants for monitoring and manipulating activity and gene expression in defined neural circuits. Neuron *71*, 617–631.

Park, J.I., Venteicher, A.S., Hong, J.Y., Choi, J., Jun, S., Shkreli, M., Chang, W., Meng, Z., Cheung, P., Ji, H., et al. (2009). Telomerase modulates Wnt signalling by association with target gene chromatin. Nature *460*, 66–72.

Rufer, N., Brummendorf, T.H., Kolvraa, S., Bischoff, C., Christensen, K., Wadsworth, L., Schulzer, M., and Lansdorp, P.M. (1999). Telomere fluorescence measurements in granulocytes and T lymphocyte subsets point to a high turnover of hematopoietic stem cells and memory T cells in early childhood. J. Exp. Med. *190*, 157–167.

Sahin, E., and Depinho, R.A. (2010). Linking functional decline of telomeres, mitochondria and stem cells during ageing. Nature *464*, 520–528.

Santarelli, L., Saxe, M., Gross, C., Surget, A., Battaglia, F., Dulawa, S., Weisstaub, N., Lee, J., Duman, R., Arancio, O., et al. (2003). Requirement of hippocampal neurogenesis for the behavioral effects of antidepressants. Science *301*, 805–809.

Sarin, K.Y., Cheung, P., Gilison, D., Lee, E., Tennen, R.I., Wang, E., Artandi, M.K., Oro, A.E., and Artandi, S.E. (2005). Conditional telomerase induction causes proliferation of hair follicle stem cells. Nature *436*, 1048–1052.

Silva, A.J., Zhou, Y., Rogerson, T., Shobe, J., and Balaji, J. (2009). Molecular and cellular approaches to memory allocation in neural circuits. Science *326*, 391–395.

Squire, L.R. (1992a). Declarative and nondeclarative memory: multiple brain systems supporting learning and memory. J. Cogn. Neurosci. *4*, 232–243.

Squire, L.R. (1992b). Memory and the hippocampus: a synthesis from findings with rats, monkeys, and humans. Psychol. Rev. *99*, 195–231.

Sudhof, T.C., Czernik, A.J., Kao, H.T., Takei, K., Johnston, P.A., Horiuchi, A., Kanazir, S.D., Wagner, M.A., Perin, M.S., De Camilli, P., et al. (1989). Synapsins: mosaics of shared and individual domains in a family of synaptic vesicle phosphoproteins. Science *245*, 1474–1480.

Vivar, C., Potter, M.C., Choi, J., Lee, J.Y., Stringer, T.P., Callaway, E.M., Gage, F.H., Suh, H., and van Praag, H. (2012). Monosynaptic inputs to new neurons in the dentate gyrus. Nat. Commun. *3*, 1107.

Wege, H., and Brummendorf, T.H. (2007). Telomerase activation in liver regeneration and hepatocarcinogenesis: Dr. Jekyll or Mr. Hyde? Curr. Stem Cell Res. Ther. *2*, 31–38.

Yuan, X., Ishibashi, S., Hatakeyama, S., Saito, M., Nakayama, J., Nikaido, R., Haruyama, T., Watanabe, Y., Iwata, H., Iida, M., et al. (1999). Presence of telomeric G-strand tails in the telomerase catalytic subunit TERT knockout mice. Genes Cells *4*, 563–572.

Zhao, C., Deng, W., and Gage, F.H. (2008). Mechanisms and functional implications of adult neurogenesis. Cell *132*, 645–660.

Zhao, Y., Sfeir, A.J., Zou, Y., Buseman, C.M., Chow, T.T., Shay, J.W., and Wright, W.E. (2009). Telomere extension occurs at most chromosome ends and is uncoupled from fill-in in human cancer cells. Cell *138*, 463–475.

Zhou, Q.G., Hu, Y., Wu, D.L., Zhu, L.J., Chen, C., Jin, X., Luo, C.X., Wu, H.Y., Zhang, J., and Zhu, D.Y. (2011). Hippocampal telomerase is involved in the modulation of depressive behaviors. J. Neurosci. *31*, 12258–12269.

Stem Cell Reports, Volume *9*

Supplemental Information

Hippocampal TERT Regulates Spatial Memory Formation through Modulation of Neural Development

Qi-Gang Zhou, Meng-Ying Liu, Han-Woong Lee, Fuyuki Ishikawa, Sushil Devkota, Xin-Ru Shen, Xin Jin, Hai-Yin Wu, Zhigang Liu, Xiao Liu, Xun Jin, Hai-Hui Zhou, Eun Jeoung Ro, Jing Zhang, Yu Zhang, Yu-Hui Lin, Hoonkyo Suh, and Dong-Ya Zhu

Supplementary Information

Hippocampal TERT regulates spatial memory formation through modulation of neural development

Qi-Gang Zhou, Meng-Ying Liu, Han-Woong Lee, Fuyuki Ishikawa, Sushil Devkota, Xin-Ru Shen, Xin Jin, Hai-Yin Wu, Zhigang Liu, Xiao Liu, Xun Jin, Hai-Hui Zhou, Eun Jeoung Ro, Jing Zhang, Yu Zhang, Yu-Hui Lin, Hoonkyo Suh, Dong-Ya Zhu

Supplemental Figures

Figure S1. Validation of the *Tert* $^{-/-}$ mice. Related to Figure 1

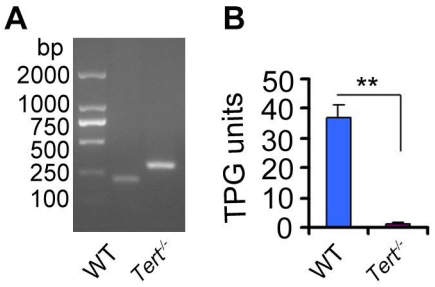

Figure S2. Latency to the platform in visible platform training**.** Related to Figure 1, 2, 6 and 7

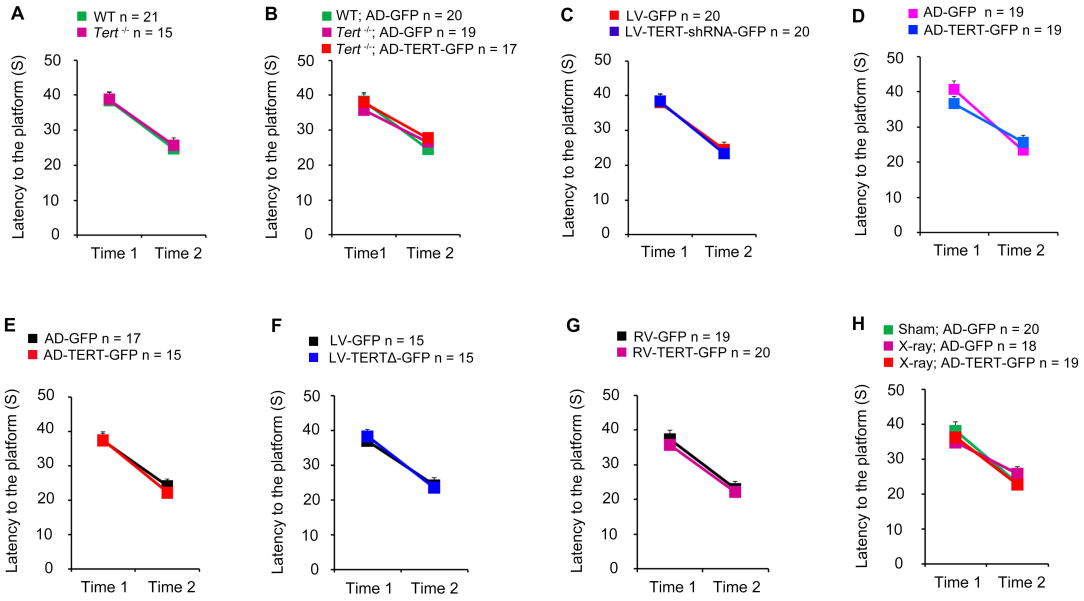

Figure S3. TERT expression dynamic induced by AD-TERT-GFP. Related to Figure 2

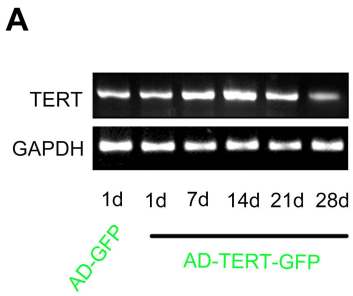

Figure S4. Validation of RV-TERT-GFP *in vivo* and *in vitro*. Related to Figure 4

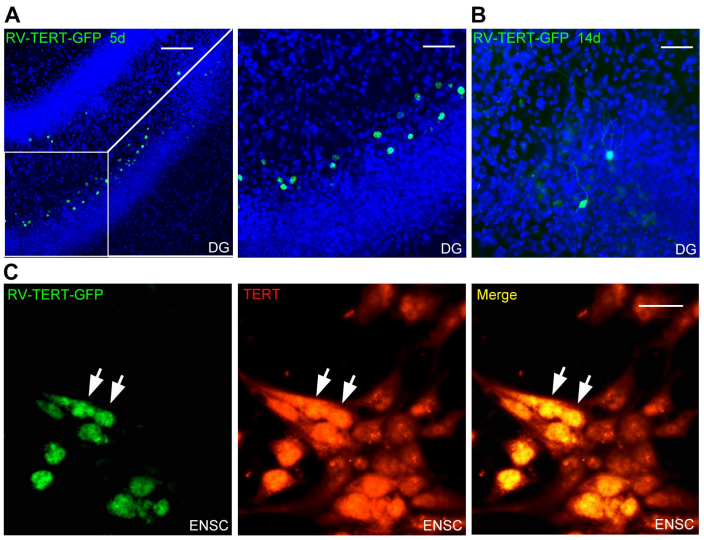

Figure S5. Cell types of LV-TERT-GFP infected cells in the DG. Related to Figure 7

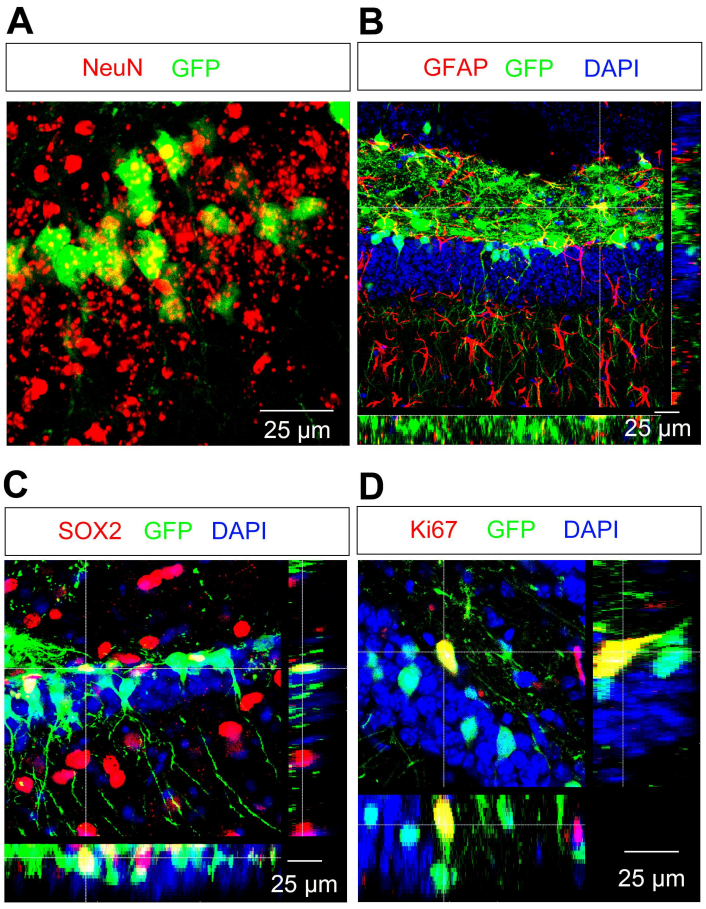

Figure S6. X ray-irradiation causes cell death selectively in the sub-granular layer of the DG. Related to Figure 7

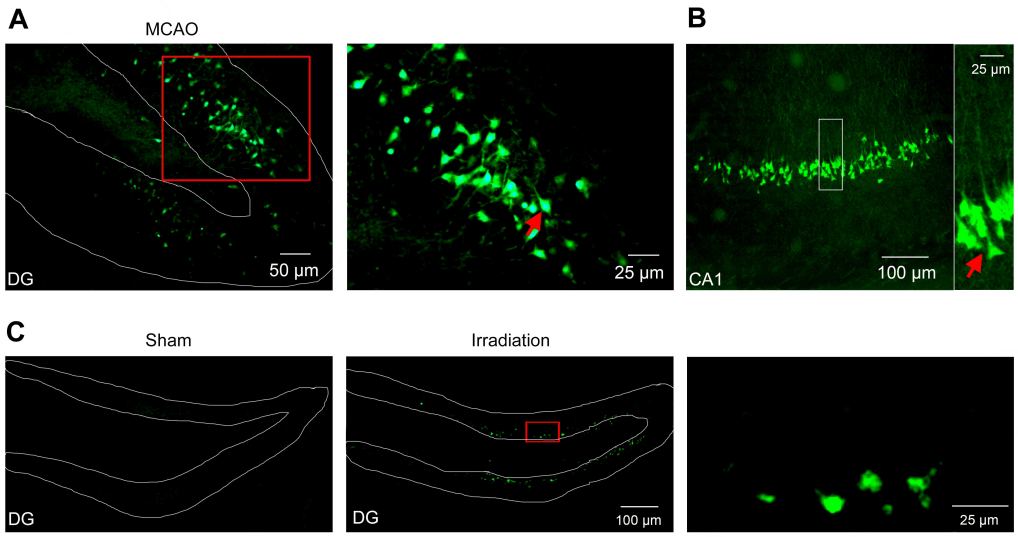

Figure S7. Expression of shortened TERT with non-activity in the DG did not cause depression-related behavior. Related to Figure 6

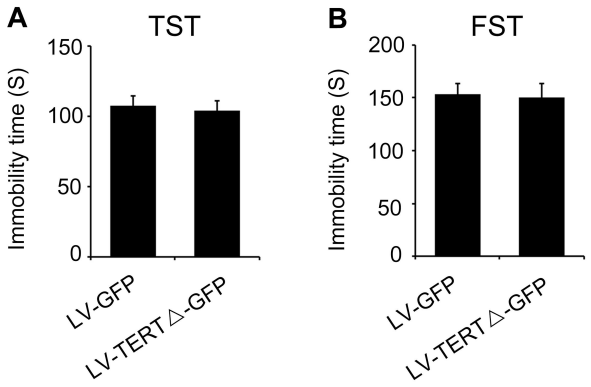

Table S1. The swimming speeds in probe test of mice in each experiment. Related to Figure 1, 2, 6 and 7

Experiments	Groups	n	Swim speed (mm/s) Mean ± SEM	*P* value
Figure 1**A**	WT	21	507.4667 ± 14.9994	0.2199
	Tert$^{-/-}$	15	479.3620 ± 16.3210	
Figure 1**E**	WT;LV-GFP	20	445.1270 ± 15.7291	0.2430
	Tert$^{-/-}$;LV-GFP	19	451.6412 ± 18.0740	
	Tert$^{-/-}$;LV-TERT-GFP	17	413.9472 ± 15.7541	
Figure 1**H**	LV-GFP	20	431.5740 ± 12.4375	0.5923
	LV-TERT-shRNA-GFP	20	420.2310 ± 16.9280	
Figure 2**A**	AD-GFP	19	452.5030 ± 22.5279	0.7358
	AD-TERT-GFP	19	442.1970 ± 20.2784	
Figure 2**B**	AD-GFP	17	457.2770 ± 9.8820	0.2354
	AD-TERT-GFP	15	441.4620 ± 15.3795	
Figure 6**E**	LV-GFP	15	439.3920 ± 10.4737	0.1592
	LV-TERTΔ-GFP	15	447.8219 ± 12.3251	
Figure 7**A**	RV-GFP	19	467.9337 ± 15.2172	0.3116
	RV-TERT-GFP	20	489.0720 ± 13.5414	
Figure 7**D**	Sham + AD-GFP	20	458.0568 ± 12.9293	0.8916
	X ray + AD-GFP	18	477.3935 ± 15.0006	
	X ray + AD-TERT-GFP	19	484.0584 ± 16.8535	

Movie S1. Related to Figure 1

This movie showed the performance of a mouse in WT group in MWM test at day 5 during 5-day training. The WT mouse found the platform in a short time.

Movie S2. Related to Figure 1

This movie showed the performance of a mouse in *Tert*$^{-/-}$ group in MWM test at day 5 during 5-day training. The *Tert*$^{-/-}$ mouse did not found the platform.

Supplemental Figure Legends

Figure S1. Validation of the *Tert* $^{-/-}$ mice (related to Figure 1). (**A**) RT-PCR showing the genotype of the *Tert* $^{-/-}$ mice. (**B**) Deletion of telomerase activity in the embryonic stem cells from *Tert* $^{-/-}$ mice ($n = 3$ independent experiments, $P = 0.0012$, Student's t-test.). Error bars, s.e.m.

Figure S2. Latency to the platform in visible platform training (related to Figure 1, 2, 6 and 7). (A) Related to Figure 1A. (**B**) Related to Figure 1E. (**C**) Related to Figure 1H. (**D**) Related to Figure 2A. (**E**) Related to Figure 2B. (**F**) Related to Figure 6E. (**G**) Related to Figure 7A. (**H**) Related to Figure 7D. One-way ANOVA in (**B** and **G**) and Student's *t*-test in the others. Error bars, s.e.m.

Figure S3. TERT expression dynamic induced by AD-TERT-GFP (related to Figure 2). (**A**) RT-PCR showing the expression dynamic of TERT mRNA after injection of AD-TERT-GFP into the DG. $n = 3$ independent experiments.

Figure S4. Validation of RV-TERT-GFP *in vivo* and *in vitro* (related to Figure 4). (**A**) Representative image of the DG infected by RV-TERT-GFP 5 days after RV infection. On the right: a high-magnification image from the box area, showing the location of RV-TERT-GFP in the sub-granular layer. (**B**) Representative image of the DG infected by RV-TERT-GFP 14 days after RV infection. Note that the major GFP fluorescence was observed in the cell body. (**C**) Representative image of the cultured NSCs infected by RV-TERT-GFP (left) with immunostaining with anti-TERT primary antibody (middle). The merge of RV-TERT-GFP signal with TERT immunostaining signal (yellow) was shown (right). Note: the signal of TERT in the NSCs infected by RV-TERT-GFP (arrow indicated) was significantly stronger than others, indicating an enhancement of TERT expression in NSCs by RV-TERT-GFP 24 hours after infection in NSCs culture. Scale bars: **A** (left), 100 μm; **A** (right) and **B**, 50 μm, **C**, 25 μm.

Figure S5. Cell types of LV-TERT-GFP infected cells in the DG (related to Figure 7). (**A**) Representative photo showing that NeuN^{+} neurons located at the granular layer were infected by LV-TERT-GFP. (**B**) Representative photo showing that GFAP^{+} astrocytes in the hillus were infected by LV-TERT-GFP. (**C**) Representative photo showing that SOX2^{+} cells located in the sub-granular layer were infected by LV-TERT-GFP. (**D**) Representative photo showing that Ki67^{+} cells located in the sub-granular layer were infected by LV-TERT-GFP.

Figure S6. X ray-irradiation causes cell death selectively in the sub-granular layer of the DG (related to Figure 7). (**A**) Representative photos showing FJ-positive cells located in the DG 7 days after MCAO. A magnification of the box area was shown on the right. Red arrow indicated that

FJ-positive cells located in the granular layer with neuronal morphology. (**B**) Representative photos showing FJ-positive cells located in the CA1 7 days after MCAO. A magnification of the box area was shown on the right. Red arrow indicated that FJ-positive cells located in the granular layer with neuronal morphology. (**C**) Representative photos showing FJ-positive cells in the DG of mice with/without exposure to irradiation. A magnification of the box area was shown on the right. Red arrow indicated that FJ-positive cells located in the granular layer with the morphology of NPCs. $n = 3$ independent experiments.

Figure S7. Expression of shortened TERT with non-activity in the DG did not cause depression-related behavior (related to Figure 6). (A) Bar graph showing the immobility time of mice in TST 28 days after injection of LV-GFP or LV-TERTΔ-GFP into the DGs. $n = 15$. $P = 0.7148$. Student's *t*-test. (B) Bar graph showing the immobility time of mice in FST 28 days after injection of LV-GFP or LV-TERTΔ-GFP into the DGs. $n = 15$. $P = 0.8810$. Student's *t*-test.

Supplemental Experimental Procedures

Genotyping

Genotyping Primers of *Tert*$^{-/-}$ mice: (1) gcg tgg agt atc ctc ctg cat ctc ta, (2) ctg tct cct aaa gga ctt gtg gac tt, (3) agg att ggg aag aca ata gca ggc at. The primer stock should be diluted to make 100 picomoles/ µl. Then mix 10 µl of each primer 1, 2, and 3 with 70 µl 3-distilled water to make final volume of 100 µl. This 100 µl is the working stock. 1 µl of the working stock can be used for 1 PCR reaction. PCR cycles: 32 cycles. Denaturation: 94 °C, 30 sec. Annealing: 55 °C, 30 sec. Extension: 72 °C, 1 min. Final extension: 72 °C, 10 min.

Virus construction

RV-TERT-GFP The sequence of TERT-GFP in the plasmid pDC315-TERT-GFP was cutted by using restriction enzymes and inserted into the plasimd pCAG-GFP (For RV-GFP) by T4 DNA ligase to replace the sequence of GFP in pCAG-GFP. GFP was fused to the C-terminal of TERT. The plasmid was named as pCAG-TERT-GFP, which was used to identify by DNA sequencing. Using 100µl Lipofectamine 2000, 293T cells were co-transfected with 22.5 µg of pCAG-TERT-GFP, 15 µg of pCMV-GP, and 7.5 µg of pCMV-VSVG to generate the recombinant retrovirus, RV-TERT-GFP. After 48 h, supernatant was harvested from 293T cells, filtered at 0.45 µ m, and pelleted by ultracentrifugation at 18000 × g for 2 h at 4 °C. After resuspension by PBS, serially diluted retrovirus was used to transduce 293T cells; 4 days later, labeled 293T cells were counted to calculate the viral titer (~ 2 × 107 transducing units/ml). As a control, we also generated a retroviral vector that expresses GFP (RV-GFP) or RFP (RV-RFP) alone.

AD-TERT-GFP Briefly, the coding sequence of mouse TERT was amplified by RT-PCR. The primer sequences were as follows: forward, 5'-GTAGAACGCAGATCGAAT-TCATGACCCGCGCTCCTCG-3'; reverse, 5 '-CCCTTGCTCACCATG-AATTCGTCCAAAATGGTCTGAAAGTC-3'. The PCR fragments and the pDC315-GFP plasmid were digested with EcoR I and ligated with T4 DNA ligase to produce pDC315-mTERT-IRES-GFP. The plasmid was used to trans-form competent DH5α Escherichia coli bacterial strains for identification. Using 100µl of Lipofectamine 2000 mixed with 50 µl of DMEM, HEK293 cells were cotransfected with 5 µg of the pDC315-GFP plasmid with a cDNA encoding mTERT and 5 µg of the pBHG lox ΔE1,3 Cre plasmid as a helper plasmid to generate the recombinant adenovirus, AD-TERT-GFP. After 8 d, supernatant was harvested from HEK293 cells. After 3 times the virus amplification, the supernatant was filtered at 0.45µm and purified using the Adeno-X Virus Purification kit. After resuspension, serially diluted adeno-virus was used to transduce HEK293 cells. Seven days later, labeled HEK293 cells were counted to calculate the viral titer (~ 2.5 × 10 10 pfu/ml). As a control, we also generated a adenoviral vector that expresses GFP alone (AD-GFP).

LV-TERT-GFP and LV-TERTΔ-GFP Briefly, the coding sequence of mouse TERT was amplified by RT-PCR. The primer sequences were as follows: forward, 5'-GTAGAACGCAGATCGAAT-TCATGACCCGCGCTCCTCG-3'; reverse, 5 '-CCCTTGCTCACCATG-AATTCGTCCAAAATGGTCTGAAAGTC-3'. The PCR fragments was cutted by restriction enzymes and inserted into the plasimd pCMV-GFP (For LV-GFP) by T4 DNA ligase to replace the sequence of GFP in pCMV-GFP. GFP was under control of another promotor pUbi. Mice mTERTΔ gene was amplified by our previous consructed plasmid LV-TERT-GFP carring the whole gene encoding TERT by deletion mutant PCR. The primer sequences were as follows: forward, 5'-GAGGATCCCCGGGTACCGGTCGCCACCATGACCCGCGCTCCTCGTTGCC-3'; reverse, 5 '-TCCTTGTAGTCCATACCGTCCAAAATGGTCTGAAAGTCTGTGCTTAG -3'. The PCR fragments and the pGV287-GFP plasmid were digested with Age 1 and BamH 1 and ligated with T4 DNA ligase to produce LV-TERTΔ-GFP. Using 100μl Lipofectamine 2000, 293T cells were co-transfected with 20 μg of pCMV-TERT-GFP, 10 μg of VSVG, 7.5 μg of RSV-REV and 3.5 μg pMDL g/p RRE to generate the recombinant lentiovirus, LV-TERT-GFP. After 48 h, supernatant was harvested from 293T cells, filtered at 0.45 μ m, and pelleted by ultracentrifugation at 18000 × g for 2 h at 4 °C. After resuspension by PBS, serially diluted retrovirus was used to transduce 293T cells; 4 days later, labeled 293T cells were counted to calculate the viral titer (~ 2 × 109 transducing units/ml). As a control, we also generated a retroviral vector that expresses GFP alone (LV-GFP).

LV-TERT-shRNA-GFP Mouse TERT shRNA (m) Lentiviral Particles, we named it LV-TERT-shRNA-GFP, and its control shRNA Lentiviral Particles (LV) were purchased (Santa Cruz, CA, USA). LV-TERT-shRNA-GFP is a pool of concentrated, transduction-ready viral pa rticles containing 4 target-specific constructs that encode 19- 25 nt (plus hairpin) shRNA designed to knock down gene expression. Each vial contains 200 μl frozen stock containing 1.0 × 106 infectious units of virus (IFU) in Dulbecco's Modified Eagle's Medium with 25 mM HEPES pH 7.3.

RV-SYN-GTR, RV-SYN-GT, and EnvA-ΔR-mCh The plasmids of RV-SYN-GTR and RV-SYN-GT were constructed based on the plasmids from Callaway's lab purchased from addgene (Osakada and Callaway, 2013). RV-SYN-GTR and RV-SYN-GT were produced by transient transfection of the RV-SYN-GTR or RV-SYN-GT vector (7.5 μg), CMVGagPol (5 μg) and CMV-VSVG (2.5 μg) in 60% confluent 293T cells grown in 10-cm plates for 5 hours. Virus-containing supernatant was harvested 48 hours later. The final titers were estimated to be ~ 2 × 107 pfu/ml or ~ 1 × 107 pfu/ml as determined by infection of serially diluted virus into 293T cells. The production of EnvA-ΔR-mCh was carried out as described previously (Osakada and Callaway, 2013; Osakada et al., 2011). Briefly, glycoprotein–gene-deleted rabies virus vector (ΔR-mCherry) was generated in which a mCherry reporter gene was replaced with the cDNA encoding the rabies virus glycoprotein. The helper cell line, BHK-EnvARGCD, was infected with ΔR-mCherry, to produce rabies virus pseudotyped with envelope protein EnvA. After 2 h and 4 h, the cells were washed with PBS three times and the media

reapplied. Supernatants containing ΔR-mCherry rabies virus pseudotyped with EnvA were harvested 5 days later, filtered and concentrated by ultracentrifugation. EnvA-ΔR-mCh titre was estimated to be ~1.2×107 pfu/ml and diluted for use to ~4×106 pfu/ml.

Western blot

Western bolt analysis of samples from cultured hippocampal neurons, NSC, and hippocampal tissues of animals was performed as described previously (Zhou et al., 2011b). The primary antibodies: Rabbit Anti-Flag (Bioss, bs-0287R), Mouse Anti-GAPDH (Kangchen Bio-Tech, kc-5G4), and Rabbit Anti-Synapsin 1 (Millipore, AB1543). Appropriate horseradish peroxidase-linked secondary antibodies were used for detection by enhanced chemiluminescence (Pierce).

MCAO

Focal cerebral ischemia was induced by MCAO, as described previously (Zhou et al., 2010). In brief, under chloral hydrate anesthesia (350 mg/kg, i.p.), a 8/0 surgical nylon monofilament with rounded tip was introduced into the left internal carotid artery through the external carotid stump, advanced 16–17 mm past the carotid bifurcation until a slight resistance was felt. At this point, the intraluminal filament blocked the origin of the middle cerebral artery and occluded all sources of blood flow from the internal carotid artery, anterior cerebral artery, and posterior cerebral artery. Throughout the procedure, body temperature was maintained at 37 ± 0.5 °C. The filament was left in place for 90 min and then withdrawn. In the sham-operated animals, the occluding filament was inserted 7 mm above the carotid bifurcation.

Fluoro-Jade staining

Neuronal degeneration and death were determined by Fluoro-Jade (FJ; Histo-Chem) staining (Zhou et al., 2011a). In brief, sections were washed and mounted on glass slides and dried overnight. The slides were immersed for 3 min in absolute ethanol solution, for 1 min in 70% ethanol solution, and for 1 min in distilled water. Then, the slides were transferred into a solution containing 0.01% Fluoro-Jade and 0.1% acetic acid for 30 mintues on a shaker. After three 10 mintues washes, the slides were finally coverslipped for analysis.

Immunocytochemistry

Mice were anesthetized with with 0.07 ml of a mixture of ketamine (90.9 mg/ml) and xylazine (9.1 mg/ml) and perfused transcardially with saline followed by about 50 ml of 4% paraformaldehyde (PFA). Brains were removed and postfixed overnight in 4% PFA. Serial sections (40μm) were made on an oscillating tissue slicer in a bath of physiological saline. Every sixth section throughout the hippocampus was processed for 5-bromo-2′-deoxyuridine (BrdU) (Rat, Bio-rad, OBT0030) immunohistochemistry as described previously. All the sections throughout the brain were collected

for tracing analyis. All the cells were counted in each section by another experimenter blinded to the study code. Other primary antibodies: Rabbit Anti-DCX (Santa Cruz Biotechnology, sc-28939), Rabbit Anti-GFAP (Abcam, ab7260), Mouse Anti-GFP (Santa Cruz Biotechnology, sc-101525), Rabbit Anti-RFP (Abcam, ab62341), Rabbit Anti-Ki67 (Abcam, ab66155), Rabbit Anti-SOX2 (Abcam, ab97959), Rabbit Anti-NeuN (Cell Signaling, #24307), and Rabbit Anti-Synapsin 1 (Millipore, AB1543).

RT-PCR

Total mRNA was extracted from the hippocampus using Trizol reagent according to the manufacturer's instructions (Sigma). The primers used for RT-PCR: TERT: forward, 5' –ATGGCGTTCCTGAGTATG – 3', reverse, 5' –AGCCAGAGGCCTTTAGT – 3'; GAPDH: forward, 5' – CAAGGTCATCCATGACAACTTTG – 3', reverse, 5' – GTCCACCACCCTGTTGCTGTAG - 3'. PCR conditions were 30 cycles of denaturation at 94°C for 45 s, annealing at 55°C for 45 s, and extension at 72°C for 45 sec. PCR products were separated by electrophoresis through 1.5% agarose gel containing 0.5% lg/mL ethidium bromide and imaged using a BioDoc-IT imaging system (Bio-Rad); band intensities were determined using GS-710 calibrated imaging Densitometer (Bio-Rad). The mRNA for GAPDH was detected as a standard.

Telomerase activity assay

Telomerase activity was detected using TRA-PEZE XL telomerase detection kit (Millipore, Billerica, MA) as described previously (Zhou et al., 2011a). Following the manufacturer's instructions, telomeric repeat amplification protocol reactions (TRAP) were performed using the TRAPEZE XL telomerase detection kits (Millipore) for analysis of the telomerase activity. The fluorescence energy transfer primers were used to generate fluorescently labeled TRAP products, quantitatively measured with a fluorescence plate reader (SpectraMax M2e) or visualized after terminal deoxynucleotidyl transferase-mediated dUTP nickend labeling on a 10% nondenaturing gel and SYBR Green I (Invitrogen) staining.

Analysis of spine density and morphology of neurons

Images of GFP-labeled neurons or DCX^+ neurons were acquired at 1 μm intervals with the Leica confocal system with a plane apochromatic 40 × oil lens and a digital zoom of 1.5. The image files were used for reconstruction of the morphology with the Imaris v7.2.3 program. The length of each dendritic segment was determined by tracing the center of the dendritic shaft, and the number of spines was counted manually from the two-dimensional projections. The linear spine density was calculated by dividing the total number of spines by the length of the dendritic segment. For classification of mushroom spines, major and minor axes of each spine head were identified. When the

width size of the spine > 0.6 μm, the spines regonized as mushroom spines. Confocal imaging and data quantification were done by the same person, who was blinded to the experimental conditions.

Stereotaxic surgery

Mice were anesthetized with 0.07 ml of a mixture of ketamine (90.9 mg/ml) and xylazine (9.1 mg/ml) and placed in a stereotaxic apparatus. Stereotaxic surgery was performed to deliver viruses or drugs into the hippocampal DG (1 μl, coordinates: 2.3 mm posterior to bregma, 1.35 mm lateral to the midline, and 2.3 mm below dura), The mice were recoverd on hot pad (37 °C) until waken up and then retrun back to homecages (Zhou et al., 2011).

Hippocampal X-irradiation

As described previously (Zhou et al., 2011), X-irradiation was performed. Briefly, mice were anesthetized with 0.07 ml of a mixture of ketamine (90.9 mg/ml) and xylazine (9.1 mg/ml). Then mice were placed in a stereotaxic apparatus and the hippocampal zone were exposed to cranial irradiation using therapeutical x-ray equipment operated at 300 kVp and 20 mA. Mice were protected with a lead shield that covered the entire body, with the exception of a 3.2 × 11 mm treatment field above the hippocampus. The corrected dose rate was ≈ 3 Gy/min at a source-toskin distance of 100 cm. The procedure lasted 1 min and 42 s, delivering a total of 5 Gy each time.

Cell Cultures

Primary hippocampal neurons were cultured from embryonic hippocampus, on embryonic day 18 (E18), of WT or *Tert*$^{-/-}$ mice in neurobasal medium (Gibco) containing 2% B27 supplement as reported (Luo et al., 2010). NSCs differentiation was also performed from embryonic hippocampus on embryonic day 18 (E18), of WT or *Tert*$^{-/-}$ mice. Monolayer-cultured NSCs were allowed to differentiate in growth factor-free DMEM/F12 (1:1) medium containing 2% B27 and 0.5% fetal bovine serum. Four days later, the cultures were fixed and stained with DCX and GFAP antibodies to mark neurons and astrocytes, respectively. The percentages of neurons and astrocytes were calculated in 10 high-power fields systematically across the coverslip.

Supplemental References

Luo, C.X., Jin, X., Cao, C.C., Zhu, M.M., Wang, B., Chang, L., Zhou, Q.G., Wu, H.Y., and Zhu, D.Y. (2010). Bidirectional regulation of neurogenesis by neuronal nitric oxide synthase derived from neurons and neural stem cells. Stem cells *28*, 2041-2052.

Osakada, F., and Callaway, E.M. (2013). Design and generation of recombinant rabies virus vectors. Nature protocols *8*, 1583-1601.

Osakada, F., Mori, T., Cetin, A.H., Marshel, J.H., Virgen, B., and Callaway, E.M. (2011). New rabies virus

variants for monitoring and manipulating activity and gene expression in defined neural circuits. Neuron *71*, 617-631.

Zhou, L., Li, F., Xu, H.B., Luo, C.X., Wu, H.Y., Zhu, M.M., Lu, W., Ji, X., Zhou, Q.G., and Zhu, D.Y. (2010). Treatment of cerebral ischemia by disrupting ischemia-induced interaction of nNOS with PSD-95. Nature medicine *16*, 1439-1443.

Zhou, Q.G., Hu, Y., Wu, D.L., Zhu, L.J., Chen, C., Jin, X., Luo, C.X., Wu, H.Y., Zhang, J., and Zhu, D.Y. (2011a). Hippocampal telomerase is involved in the modulation of depressive behaviors. The Journal of neuroscience : the official journal of the Society for Neuroscience *31*, 12258-12269.

Zhou, Q.G., Zhu, L.J., Chen, C., Wu, H.Y., Luo, C.X., Chang, L., and Zhu, D.Y. (2011b). Hippocampal neuronal nitric oxide synthase mediates the stress-related depressive behaviors of glucocorticoids by downregulating glucocorticoid receptor. The Journal of neuroscience : the official journal of the Society for Neuroscience *31*, 7579-7590.